Fast and tight control of motor vigor by accumulated decision evidence

Manuel Molano-Mazón[1,2,3,5], Alexandre Garcia-Duran[2,3], Jordi Pastor-Ciurana[1,3], Lluís Hernández-Navarro[1], Lejla Bektic[1], Debora Lombardo[1], Jaime de la Rocha[1,4,5], Alexandre Hyafil[2, 4, 5]

1. IDIBAPS, Rosselló 149, Barcelona, 08036, Spain
2. Centre de Recerca Matemàtica (CRM), Bellaterra, Spain
3. These authors contributed equally
4. These authors contributed equally
5. Corresponding author

Abstract

Acting in the natural world requires not only deciding among multiple options but also converting decisions into motor commands. The link between the dynamics of decision formation and the kinematics of response movement remains poorly understood. Here we investigate how the accumulation of decision evidence shapes response trajectories in a task where freely-moving rats combine prior expectations and acoustic information to select between two possible options. Rats' trajectories extracted from automatic video analysis showed that the vigor of rats' movements was initially set by the prior expectations. Rats incorporated the stimulus information after the response onset by speeding their response if the stimulus supported their choice, slowing it otherwise, or even reversing their initial trajectories to head to the alternative port when the stimulus clearly contradicted the initial choice. A remarkably similar behavior was found in humans performing an analogous task under time pressure. We encapsulated this behavior in a computational model that describes the mapping between the dynamics of evidence accumulation and the full response trajectory. The model replicates the subjects choices, response trajectories and explains the conditions yielding trajectory reversals. Together, our results show the tight and graded relationship between the evidence accumulated during perceptual decisions and the kinematics of the response trajectories described by rats and humans to execute their choices.

Introduction

Grabbing an apple at the grocery store requires not only selecting the best one, but also planning the arm's trajectory to reach it. In recent years, the classical view of a brain that works serially, first deciding what to do and then deciding how to do it, has been revised in favor of a perspective that describes these two processes as running in parallel (Gallivan et al. 2018; Wispinski, Gallivan, and Chapman 2020). This novel framework allows not only to predict motor features (the *how to do it*) from cognitive variables (that determine *what to do*), but also to leverage the study of motor kinematics to dissect the cognitive processes underlying the production of a given behavior (Seideman, Stanford, and Salinas 2018; Korbisch et al. 2022).

Motor responses supporting a choice have been characterized by their speed of execution (i.e. vigor), and by the existence of changes in motor plans along their execution (i.e. trajectory updates). Vigor is linked to the subjective value of the chosen option (Shadmehr et al. 2019), increasing with reward, both in reaching (Summerside, Shadmehr, and Ahmed 2018) and saccadic (Milstein and Dorris 2007; Xu-Wilson, Zee, and Shadmehr 2009) responses. Vigor is also impacted by urgency signals in monkeys (Thura et al. 2014) and humans (Thura 2020). However, the effect on response vigor of cognitive factors such as the evidence towards the decision is poorly understood.

Trajectory updates have been observed when decision evidence is presented sequentially and can be incorporated into an unfolding trajectory (Song and Nakayama 2009; Stone, Mattingley, and Rangelov 2022). Monkeys (Kiani et al. 2014; Kaufman et al. 2015) and humans (Resulaj et al. 2009; van den Berg et al. 2016) often reverse an initial choice if it is contradicted by novel sensory evidence (change of mind, CoM). Yet, we do not know if this online updating of trajectories represents an isolated phenomenon that only occurs when new evidence promotes a categorical change in the initial choice. Alternatively, trajectories would be constantly updated based on any novel relevant information, even if the endpoint is not affected. Where the brain operates between these two opposite scenarios has yet to be unveiled.

Computational models such as the Drift-Diffusion Model (DDM) have greatly contributed to our understanding of the internal processes that control decision-making (Roger Ratcliff and McKoon 2008). The DDM summarizes the evidence supporting the different options into a *decision variable* that evolves in time until it reaches a bound that determines the choice. This intuitive paradigm generates precise predictions about how choices and reaction times depend on stimulus evidence (R. Ratcliff 1985; Palmer, Huk, and Shadlen 2005; Bogacz et al. 2010; Pardo-Vazquez et al. 2019) and prior expectations (Urai et al. 2019; Bogacz et al. 2006; Roger Ratcliff and McKoon 2008). Recent work has extended the DDM to account for proactive responses, whereby rats and humans initiate their response at a time that is independent of the stimulus (Hernández-Navarro et al. 2021; Hawkins and Heathcote 2021). Importantly this extended model implies that, during these proactive responses, subjects incorporate the stimulus information into their response trajectories as they are being executed. However, the DDM and its extensions do not characterize either the response trajectories nor the nature, extent and timing of any interaction between decision variables and trajectory kinematics. Bridging the gap between the internal decision dynamics and the

precise movement kinematics requires the development of new models that, capitalizing on the explanatory power of accumulation models, can ultimately describe time-resolved response trajectories.

Here we investigate in rats and humans how the dynamics of evidence accumulation impact the response trajectories in a prior-guided auditory discrimination task. We track the subjects' trajectories, and find that response vigor is modulated by the amount of accumulated decision evidence provided both by the prior and the stimulus. Subjects often incorporate the sensory evidence into their ongoing response trajectory, by adjusting its vigor or by reverting the planned choice when sensory evidence strongly contradicts the initial decision. We encapsulate these observations in a new computational model that simulates both the dynamics of evidence accumulation and the response execution. When fitted to subject behavior, the model provides a parsimonious description of the relationship between these two processes, in particular the impact of the accumulated evidence on the response vigor and the conditions yielding changes-of-mind. Altogether, our results show that the evidence accumulated during perceptual decisions controls the kinematics of the response trajectory, updating them en route as new evidence arrives.

Results

Movement time depends on decision-making variables

We investigated how response trajectories are formed as rats (Groups 1 and 2; n=15; see Methods) integrate decision evidence in a perceptual task where decisions are guided both by an acoustic stimulus and the recent trial history (Hermoso-Mendizabal et al. 2020a) (Figure 1a). On each trial, following a 300-ms fixation period, a stimulus was played from two lateral speakers until the animal poked out from the center port and headed towards one of two side ports. Rats were rewarded if they selected the port associated with the louder speaker (Pardo-Vazquez et al. 2019). The stimulus strength was manipulated by varying the intensity difference between the two speakers. Moreover, trials were organized into repeating and alternating contexts, in which the probability that the stimulus category (i.e. Left vs Right) is the same as in the previous trial was 0.8 and 0.2, respectively (Figure 1a). Rats leveraged these serial correlations in the trial sequence by building a prior expectation of the next rewarded port based on the recent history of responses and outcomes (Hermoso-Mendizabal et al. 2020b). We estimated on each trial the magnitude and category of this subjective prior, a variable we called *prior evidence*, by fitting a logistic regression model (see Methods). Rats' final choices combined the prior evidence, accumulated across several trials, and the stimulus evidence, available at each trial and integrated over tens of milliseconds (Figure 1b). Importantly, in our experimental paradigm, the initiation of rat responses was often driven by a proactive process, leading to a large fraction of reaction times (RTs) that were too short to be triggered by the stimulus: express responses, defined as having RT< 50 ms, were observed in 34.3 ± 12.2% of all trials (mean±SD; Figure 1c) (Hernández-Navarro et al. 2021). Despite this independence of the response onset on the stimulus, the final choice made by the rat integrated the stimulus evidence as demonstrated by the increase in accuracy with stimulus strength (Figure 1d). This implies that in a large fraction of trials, rats process the stimulus and update their decision while moving, somewhere between the central port and the lateral port. We therefore set out to

characterize the differential impact of prior and stimulus evidence onto rats' response trajectories.

We first asked whether the decision variables prior evidence and stimulus evidence impacted the response vigor, which we identified as the velocity with which rats executed their response orienting movements to the side ports. We computed in each trial the Movement Time (MT), defined as the time between the poke out from the center port and the poke in in a lateral port (Figure 1a). To isolate the contribution of the prior evidence on vigor, we introduced *silent catch trials,* where no acoustic stimulus was played (Group 2, n = 6, mean±SD 6.7 ± 0.6% of all trials), so that rat behavior was solely based on the prior evidence. Importantly, the prior evidence impacted the vigor oppositely depending on the final response: a strong prior congruent with the response, i.e. pointing towards the selected port, shortened MT (congruent prior; Figure 1e), whereas when the prior evidence was incongruent with the response, i.e. pointed against the selected port (incongruent prior), the animal took longer. We then analyzed the impact of stimulus evidence on the movement time, restricting the analysis to trials with small prior magnitude (see Methods). Similarly to the impact of prior evidence, rat movement responses were faster when the stimulus supported the selected port (congruent stimulus), and slower when the stimulus contradicted it (incongruent stimulus; Figure 1f). When assessed altogether, MT depended on a linear combination of stimulus and prior evidence towards the response (Figure 1g-h). This influence was present in addition to a within-session slowing due to satiation and tiredness (Supp. Figure 1) (Hernández-Navarro et al. 2021). The results discussed above highlight the relative impact of congruent versus incongruent stimuli. Subsequently, we investigated whether the net effect of the stimulus on MT was positive or negative. For this, we compared MTs in silent trials and in standard trials with sound and found that MTs decreased for congruent stimuli, but increased when the stimulus was at odds with the final choice (Figure 1i). This shows that, on average, incongruent stimulus evidence effectively slowed the response originally planned. In summary, the time taken by the rats to perform a response trajectory in a decision-making task displays clear signatures of the decision making variables.

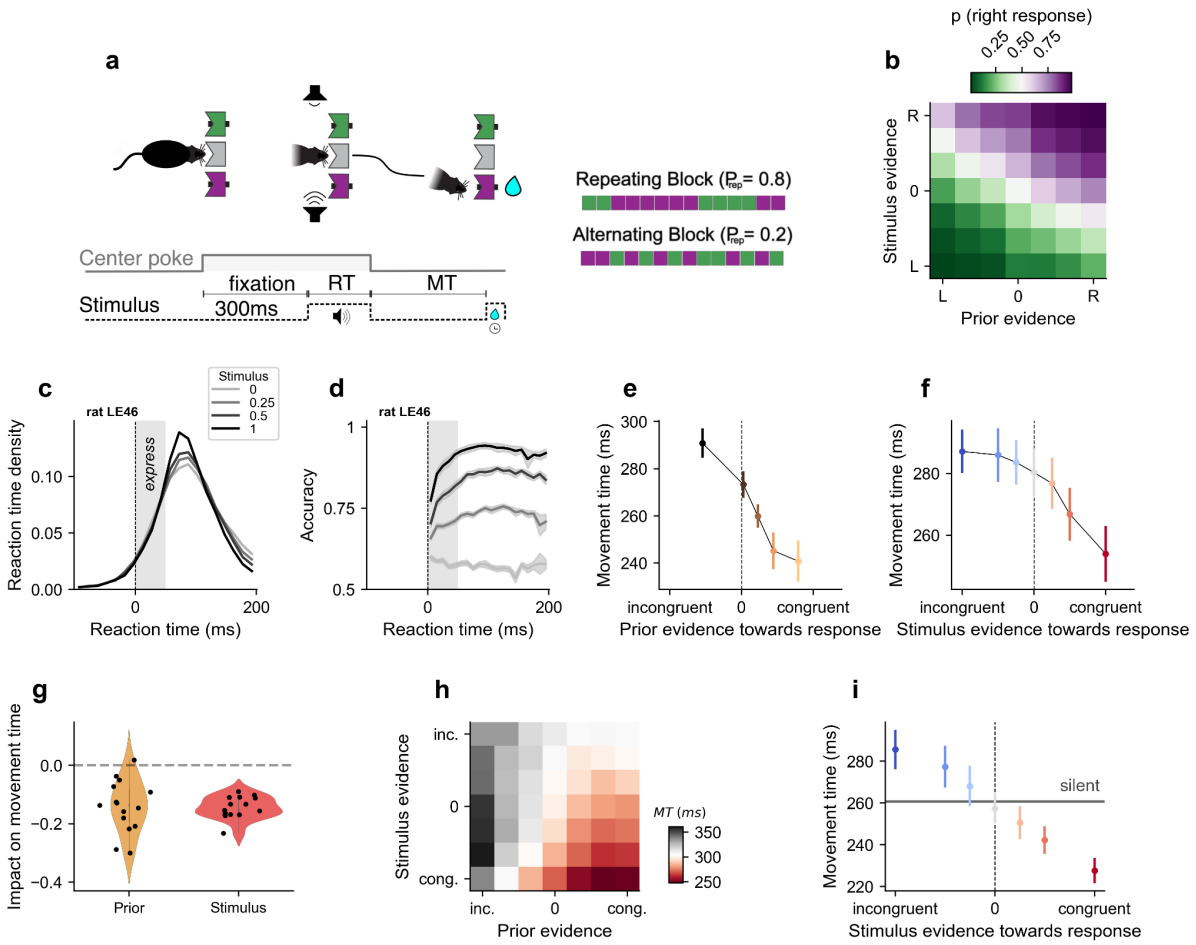

Figure 1. Rats reaction times, choices and motor times in an auditory, prior-guided, two-alternative categorization task. **a)** On each trial, rats fixated for 300 ms in the center port before an acoustic stimulus was played from two lateral speakers. Rats were free to initiate a response toward a lateral port at any time following stimulus onset. RT: reaction time defined from stimulus onset to initiation of rat response (central port withdrawal); MT: movement time defined from response initiation to the lateral port entering) **Right**:Trials are organized into blocks of 80 trials, with the probability of repeating the trial category set to P_{rep}=0.8 in repeating blocks and P_{rep}=0.2 in alternating blocks. **b)** Psychometric curve showing the proportion of rightward responses as a function of stimulus evidence (i.e. signed stimulus strength) and prior evidence, averaged across animals (Groups 1+2, n=15). **c)** Distribution of reaction times for each stimulus strength, for one typical animal (LE46). Negative RTs correspond to fixation breaks. Shaded area represents express responses (RT<50 ms). **d)** Tachometric curve representing the mean accuracy as a function of RT for the different stimulus strengths, for the same animal. **e)** Median movement time averaged across animals in silent catch trials as a function of prior evidence towards the selected port (e.g. positive if the prior points towards the animal decision and negative otherwise; binned in 5 quantiles). Error bars: standard error of the mean (s.e.m.). **f)** Median movement time in express response trials (RT< 50 ms) with small prior (|z| < 10% percentile), as a function of stimulus evidence towards the selected port. **g)** Regression weights of the movement time against the prior and stimulus evidence towards the response (see Methods). **h)** Mean movement time as a function of prior and stimulus evidence towards the selected port, averaged across animals. **i)** Average movement time as a function of stimulus evidence supporting the decision, in express response trials (RT<50 ms) with prior evidence supporting the decision (prior evidence towards response z > median). Stimuli can both accelerate or slow down the default trajectory obtained in silent trials with the same prior (dashed line).

Prior and stimulus evidence impact rats' trajectory at different times

To better characterize the dynamic interplay between cognitive factors such as prior and stimulus evidence and the unfolding motor response, we next studied the exact timing of the impact of these factors on time-resolved response trajectories. We extracted the response trajectories described by the rats during the task from video recordings of a camera placed above the animal. Using an automatic pose estimation method (Mathis et al. 2018), we inferred the coordinates of the snout of the rat in the horizontal plane, for each video frame (Figure 2a; see Methods). We focused our analyses on the dimension aligned with the three ports (Figure 2b), since it contains the most relevant information about the response orienting trajectory. Trajectories along this axis revealed relatively stereotyped movements consisting in smooth sigmoidal-like curves starting at the central port and ending at one of the side ports (Figure 2c). Consistent with the dependency of MT on prior and stimulus evidence, the analysis of the full trajectories revealed that these two decision variables accelerated or decelerated the trajectories depending on their congruence with the final choice (while preserving the same stereotyped shape) (Figure 2d, e). The peak velocity of the animal's movement reflected the prior and stimulus evidence towards the selected port (Figure 2f, g).

As expected, the impact of prior evidence onto trajectories occurred earlier than the impact of stimulus evidence (Figure 2d-g). While the prior information is available at the trial start and can in principle impact the trajectories from the response onset, sensory evidence must be integrated as the stimulus is played. Thus, the precise timing of the stimulus impact hinges on the duration of the sensorimotor processing pipeline that includes the afferent (sensory) delay, evidence integration and efferent (motor) delays. To finely quantify the onset of this impact, we computed the splitting time of trajectories, defined as the earliest time point from the stimulus onset at which the stimulus strength started affecting the trajectory (Figure 2h; see Methods). The splitting time naturally depends on the reaction time, which constrains how much processing can be done along the sensorimotor pathway before the animal pokes out from the central port. At long RTs, animals have time to accumulate enough stimulus evidence, form a decision and command a specific movement. Hence trajectories split immediately after poking out, implying that the splitting time should approximate the reaction time, after a fixed minimal delay required to detect the difference in the trajectories (Figure 2i). In contrast, at short RTs, the splitting time reaches a plateau: no matter how early the animal leaves the port, it needs a minimal amount of time before incorporating stimulus evidence into the trajectory. This minimum splitting time occurred less than 100 ms after stimulus onset (96.6 ± 25.1 ms across animals), and could be as low as 60 ms in some rats. At very small RTs (RT<10 ms), the stimulus is so short that its impact on the trajectory vanishes, causing larger splitting times. On the other hand, the prior information modulated the position of the animal even before it left the central port (Fig. 2j, right panel). Interestingly, rats prepared their response while inside the central port, by placing their snouts opposite to the side they planned to choose: the prior evidence and animal position are negatively correlated before the animal leaves the port, and become positively correlated right after leaving the port. Therefore the trajectories of the rats towards the lateral ports were influenced by prior expectations already from their initial position and by stimulus evidence as early as 60 ms after stimulus onset, reflecting the difference in availability of these two sources of information.

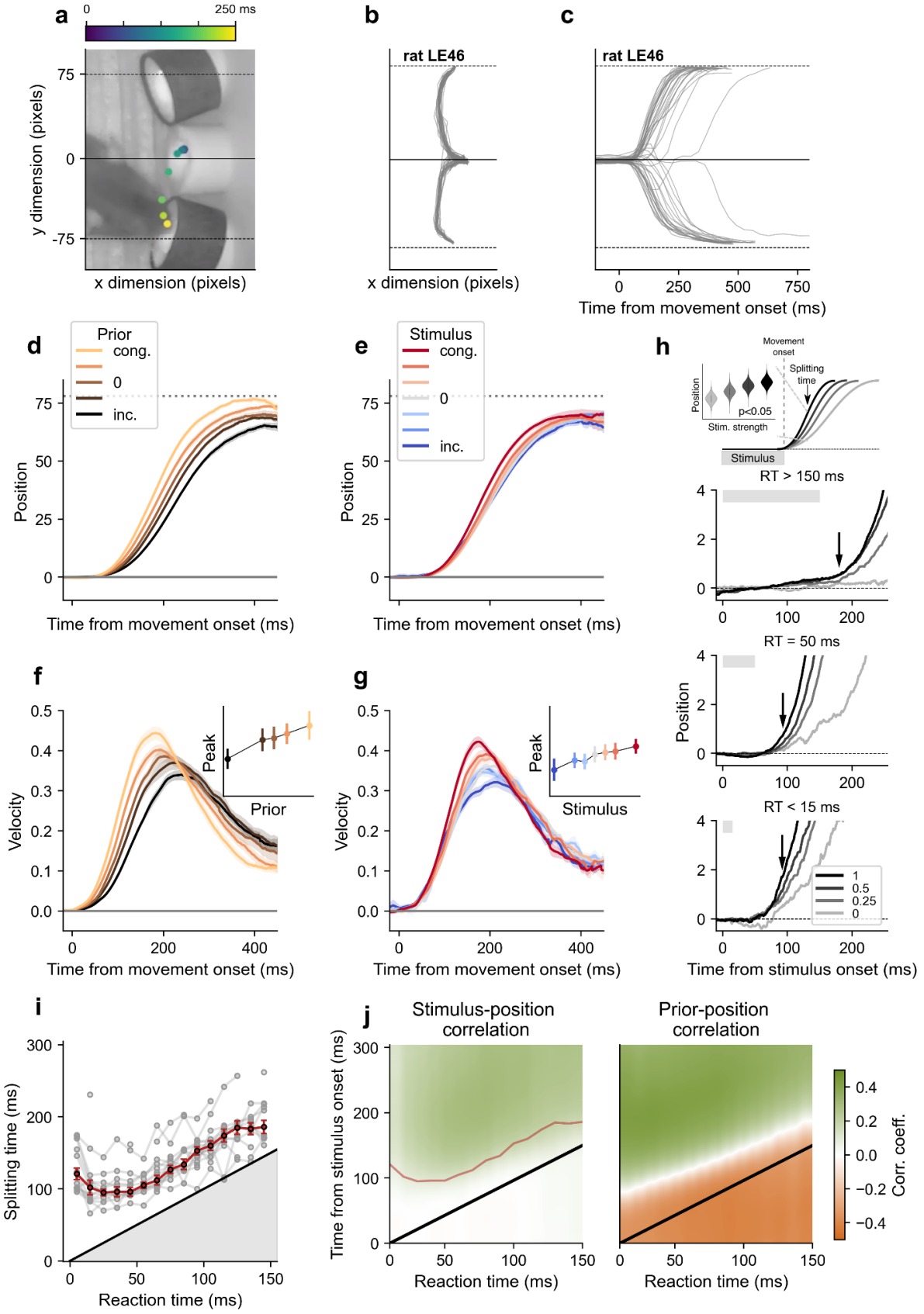
a
0
250 ms
y dimension (pixels)
x dimension (pixels)
b
rat LE46
x dimension (pixels)
c
rat LE46
Time from movement onset (ms)
d
Prior
cong.
0
inc.
Position
Time from movement onset (ms)
e
Stimulus
cong.
0
inc.
Position
Time from movement onset (ms)
h
Movement onset
Splitting time
Position
p<0.05
Stim. strength
Stimulus
RT > 150 ms
RT = 50 ms
RT < 15 ms
Position
1
0.5
0.25
0
Time from stimulus onset (ms)
f
Velocity
Peak
Prior
Time from movement onset (ms)
g
Velocity
Peak
Stimulus
Time from movement onset (ms)
i
Splitting time (ms)
Reaction time (ms)
j
Stimulus-position correlation
Prior-position correlation
Time from stimulus onset (ms)
Reaction time (ms)
Reaction time (ms)
Corr. coeff.

Figure 2. Rats' response trajectories are modulated by both prior and stimulus evidence. **a)** Example video frame showing the rat entering the right lateral port. The position of the rat snout obtained from the automatic video analysis for 6 frames prior to the frame shown is indicated by colored dots (colors correspond to the time elapsed since movement onset, see colorbar). **b)** Raw trajectories. Dashed lines as in panel a**. c)** Position of the rat along the y-dimension as a function of time from movement onset. Dashed lines as in panels a, b. **d, f)** Average position (d) and velocity (f) in silent trials as a function of time from movement onset and prior evidence towards the selected port. Inset in f: average peak velocity versus prior. Trajectories corresponding to rightward responses were flipped along the y axis so that all trajectories end at a positive value. **e, g)** Average position (e) and velocity (g) conditioned on stimulus evidence in express response trials with small prior. Inset in g: average peak velocity peak versus stimulus evidence. **h) Top:** Splitting time indicates the time at which the average trajectories are significantly affected by the stimulus, yielding a significant correlation between stimulus strength and rat position (see Methods). **Bottom:** Average trajectories for each stimulus strength, conditioned to different RT lengths: very short (RT<25 ms, bottom), medium (RT between 45 and 55 ms, middle) or very long (RT>150 ms, top) reaction times, for one example animal. Panels d, f show averages across rats for Group 2 (n=6) and panels e, g-j, for Groups 1 (n=9) and 2 (n=6). Error bars in d-g (bands). **i)** Splitting time for stimulus evidence as a function of RT (bins of 10 ms; red trace: median over rats, n=15; gray traces: individual rats; error bars: s.e.m.; RT bins were 10 ms). Shaded area corresponds to times before the rats poked out of the central port. **j)** Correlation coefficient between the position of the animal and either the stimulus evidence (left panel) or the prior evidence (right panel), as a function of the reaction time (x-axis) and time from stimulus onset (y-axis). Correlation coefficients were averaged across animals. The red curve in the left panel represents the average splitting time (see panel i). The black line represents the RT.

Incongruence between the prior and stimulus evidence leads to trajectory reversal

The above results show that trajectories, far from being predefined ballistic movements, are dynamically sped up or slowed down during their execution in response to new sensory evidence. Importantly, previous studies in humans and non-human primates have shown that fluctuations in the stream of sensory evidence can lead to changes of mind (CoMs), i.e. a change in the response trajectory towards the option that is aligned with the most recent evidence (Resulaj et al. 2009; Kiani et al. 2014; van den Berg et al. 2016; Boyd-Meredith et al. 2022). We wondered whether, in our task, stimuli strongly incongruent with the prior-guided initial trajectory could lead rats to perform CoMs, instead of simply slowing down the response without affecting the target port. We identified possible CoMs by selecting trials where the trajectory crossed a fixed threshold towards one of the lateral ports but ultimately reversed and reached the opposite port (Figure 3a-b). This procedure detected 31277 trajectory reversals across all rats (Groups 1 and 2, n = 15), which represent a low but systematic percentage of all trials (2.37 ± 0.95 %, mean±SD across animals; Figure 3b, inset). Although this percentage was sensitive to the value of the threshold used to identify the reversals, the following characterization was not. Trajectory reversals were associated with a stereotyped movement showing a standard initial trajectory towards one side followed by a clear deflection towards the final choice (Figure 3c). The reversal point of the trajectory took place on average 189 ± 15 ms after movement onset and was rarely further than 10 pixels away from the central port (i.e. less than 15% of the distance between central and lateral ports), meaning that rats reversed their trajectories when they had not departed too far from the central port (Figure 3d). Movements associated with a trajectory reversal were

on average 129 ms longer than non-reversal responses (Figure 3e), reflecting the time cost associated with longer pathways and the change of direction inherent to those trials.

Several characteristics of the trajectory reversals demonstrate that they corresponded to changes of mind, whereby a first decision driven by the prior evidence is later switched based on sensory evidence contradicting it. First, trajectory reversals were usually corrective, i.e. they amended a mistake incurred by the animals' initial decision, and they were more likely to be so for stronger stimuli (Figure 3f) (Resulaj et al. 2009). Second, trajectory reversals emerged usually when the prior and stimulus were contradictory and the initial response was aligned with the prior while the final response was aligned with the stimulus (Figure 3g), consistently across rats (Supp. Figure 2). Finally, reversals were more frequent for short RTs (Figure 3h), when the trajectory was initiated too soon to be influenced by sensory information and thus was based only on prior information. In summary, rat orienting responses are routinely updated based on incoming sensory information, which either modulates the response vigor (Figure 2) or causes a complete reversal of the initially selected choice (Figure 3).

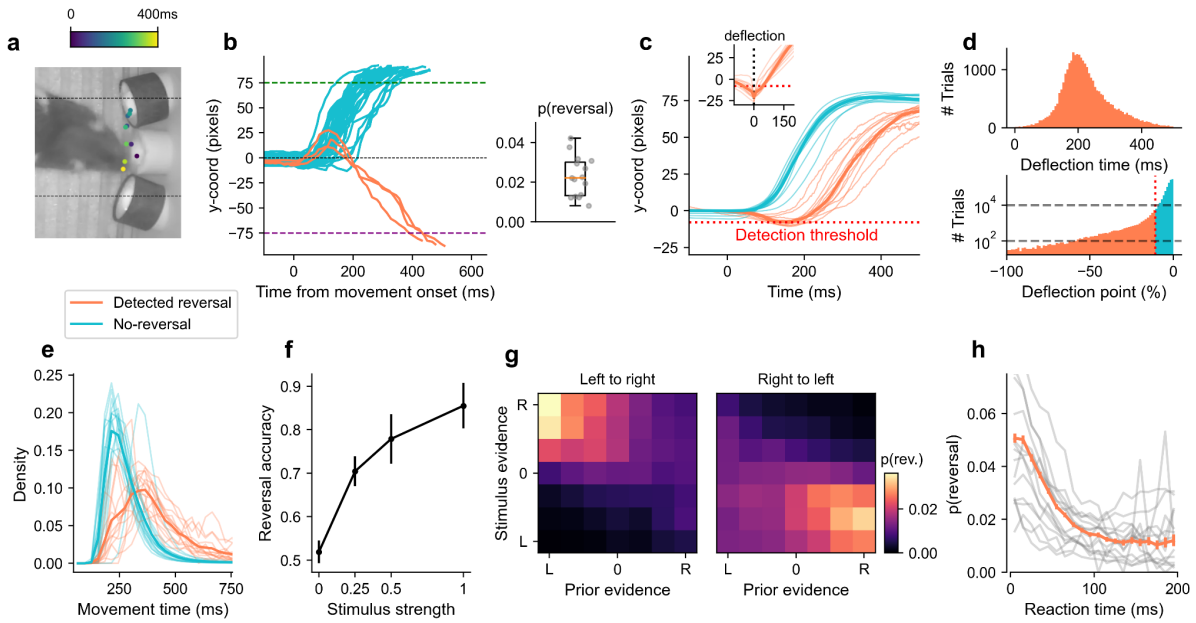

Figure 3. Rats reverse incorrect, prior-driven, initial responses based on incoming sensory information. **a)** Example video frame in a reversal trial: the rat initiates a response to the left port but then reverses and heads towards the right port. Legend as in Figure 2a. **b)** Reversal trajectories (orange traces) and standard trajectories (i.e. no reversal, blue traces) showing the position of the animal snout along the y-axis across time, from an example session. Response ports are represented with dashed lines. Right: Proportion of reversals for individual rats (Groups 1-2, n=15). **c)** Average trajectories for reversal and standard trajectories aligned at movement onset for individual animals (thin lines) and averaged across animals (thick lines). Inset: average trajectories for reversal aligned to the deflection point. Red dashed line indicates the reversal threshold used to detect reversals (8 pixels). **d) Top:** Distribution of the reversal time defined as the time from motion onset to the reversal point. **Bottom:** Histogram of the deflection point position, i.e. the maximum distance, from the central port to the deflection point (expressed as a percentage of the distance from the central to the lateral ports), obtained from all animals. Trials with deflection larger than the reversal threshold (vertical red

dashed line) are marked as trajectory reversals. **e)** Distribution of movement time for reversal (orange) and standard trajectories (blue) shown for individual animals (thin) and averaged across animals (thick). **f)** Mean choice accuracy of reversal trials as a function of stimulus strength averaged across animals. **g)** Proportion of left-to-right reversals (left) and right-to-left reversals (right) as a function of stimulus and prior evidence (binned in quantiles), averaged across animals. **h)** Proportion of reversals as a function of reaction time (gray traces: individual rats; orange trace: mean ± s.e.m.).

Human response movements also display modulation by decision processes

We next wondered whether these results generalize across species. We instructed a group of human subjects (*n*=13) to perform an intensity discrimination auditory task that closely mimicked the rat paradigm (see Methods). Briefly, subjects reported their response by sliding their finger on a tablet from a fixation point to one of two possible targets (Figure 4a-b). As in the design of the rats' task, the probability of repeating the previous trial category varied between Repeating and Alternating blocks (changes of blocks were not cued), so participants could leverage on the recent trial history to generate prior expectations about the correct side in the incoming trial (Supp. Figure 3a). We explicitly inserted an urgency component into the task, forcing subjects to initiate their response within 300 ms after stimulus onset.

Human behavior in the task was remarkably similar to that of rats. First, subjects' decisions combined the prior and sensory information (Figure 4c), and their accuracy increased with stimulus strength even for responses initiated less than 50 ms after stimulus onset (Figure 4d). Second, the movement time depended on both prior evidence and stimulus evidence: response trajectories were faster or slower depending on the congruence of these variables with the final response (Figure 4 e-f). Third, the stimulus evidence started impacting the trajectory no less than 200 ms after stimulus onset, irrespective of the reaction time (Figure 4g-h). As in rats, the splitting time was actually slightly smaller for moderate reaction times (around 200 ms) compared to very short reaction times. Fourth, we could detect a reliable proportion (7.25 ± 3.55 %, mean±SD across subjects) of trajectory reversals, which were revealed by a deflection in the response trajectory occurring around 156 ± 71 ms after movement onset (Figure 4 i-k) - more than 100 ms earlier than observed in (Nakahashi and Cisek 2023). Similar to rats, reversals occurred more often when the prior provided strong evidence towards one side but the stimulus indicated the opposite side, correcting the decision *en route* (Figure 4l); and were often associated with short RTs (Supp Fig 3b). Overall, rats and humans show a very similar relationship between the variables influencing a decision and its actual execution.

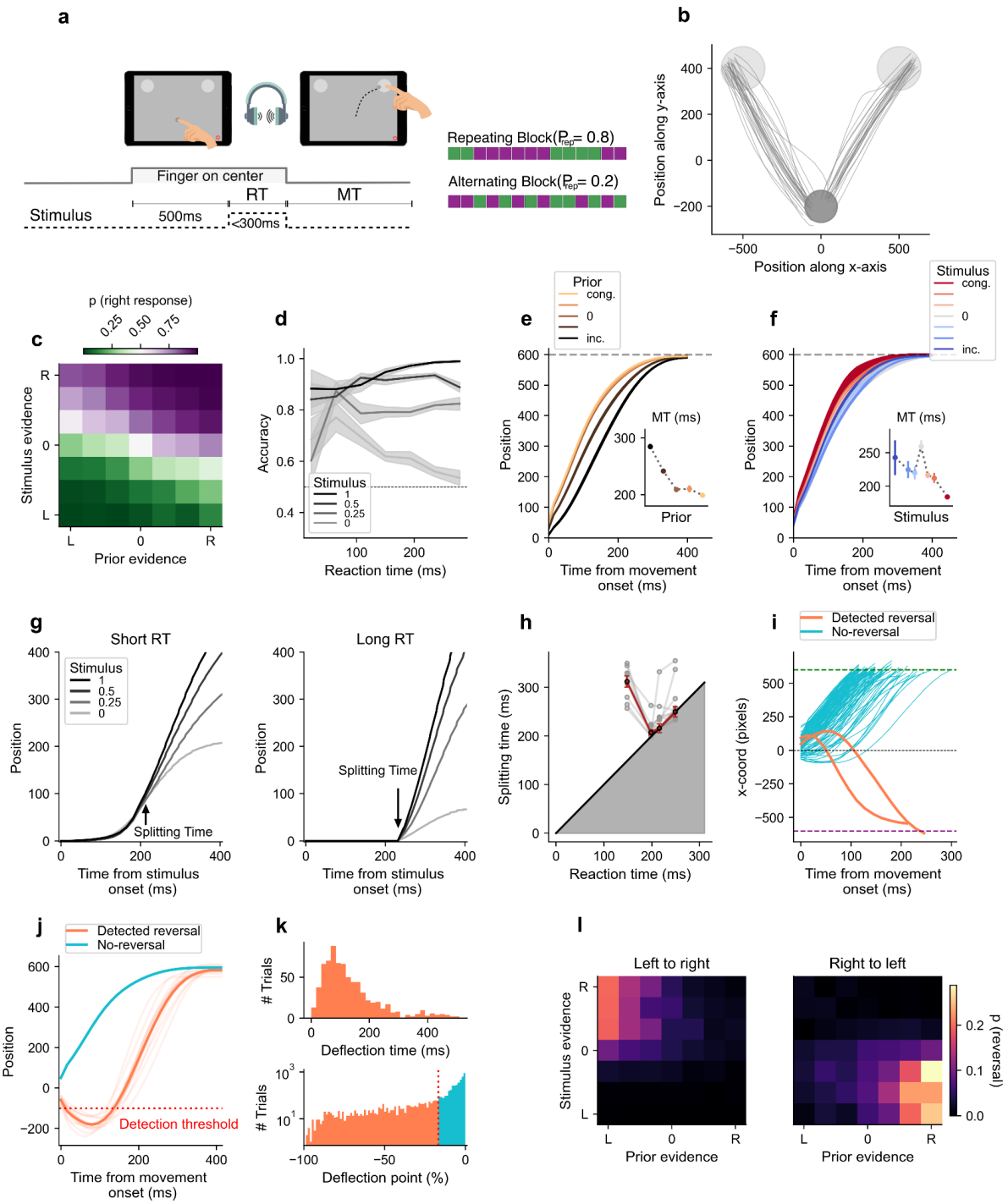

Figure 4. Human response trajectories exhibit characteristics analogous to those observed in rats. **a)** Behavioral paradigm. In each trial, human participants wearing headphones (n=13) maintained their index finger fixed on the fixation center circle of a tablet during 500 ms. An acoustic sound was then played through headphones. The participants had to initiate a trajectory along the tablet no later than 300 ms after stimulus onset and reach for one of the two target circles based on the categorization of the interaural level difference of the stimulus. **b)** Example trajectories from a typical session. **c)** Psychometric curve showing the proportion of rightward responses as a function of stimulus evidence and prior evidence, averaged across subjects (as in Fig. 1b). **d)** Mean accuracy as a function of RT for the different stimulus strengths (as in Fig. 1d). **e)** Average trajectory as a function of prior evidence. Inset: Average movement time as a function of prior evidence towards the selected port, as in Figure 1e. Legend as in Figure 2d. **f)** Average trajectory as a function of stimulus evidence for low

prior trials. Inset: Average movement time across trials as a function of stimulus evidence towards the selected port, as in Figure 1f. Legend as in Figure 2e. **g)** Average trajectories at each stimulus strength, obtained from short RT trials (first tercile, left) and long RT trials (third tercile, right). **h)** Splitting time computed for each quartile of RT, for each subject individually (gray), and averaged across subjects (red trace; error bar: s.e.m.). **i)** Example trajectories for one participant, showing standard (blue) and reversal (orange) trajectories. Legend as in Figure 3c. **j)** Average trajectory for standard trials and trajectory reversal trials. **k)** Distribution of reversal point position and reversal time across participants. **l)** Proportion of trajectory reversals as a function of prior and stimulus evidence, averaged across participants. Legend as in Figure 3g.

A parallel model of decision-making and motor trajectories

Our observations show that humans and rats initiate a first movement towards one of the lateral ports using the information available at that moment, and later update their trajectory based on new incoming sensory evidence. We formalized these ideas into a computational model that ties mechanistically the dynamics of a latent decision variable with the animal's orienting trajectory (Figure 5). The model sets apart from traditional decision-making models by fully describing the dynamics of the orienting response, and not just its end point. It consists of a decision-making module and a motor module. The decision-making module extends the classical Drift-Diffusion Model whereby a decision variable $x(t)$, initialized at a value proportional to the prior evidence, integrates sensory evidence over time until one of two decision bounds is reached and the associated response is initiated (Good 1979; Gold and Shadlen 2007; Roger Ratcliff and McKoon 2008; Urai et al. 2019; Gupta et al. 2023; Wald 2004). Following our previous work, the model includes a process linked to urgency that can also initiate movement independently of the decision variable (Hernández-Navarro et al. 2021). Thus, this process accounts for the existence of responses initiated before the integration process reaches any of the two decision boundaries (i.e. express responses, Figure 1c). Regardless of which process triggers the movement onset, the direction and vigor of the initial response is set by the value of the decision variable: the more evidence towards the selected port, the faster is the trajectory (Figure 5b). We refer to this as the first read-out (Figure 5a, empty circle). Importantly, due to sensorimotor delays, the latest sensory information is still in the processing pipeline at the moment of movement onset and thus cannot inform this response (Resulaj et al. 2009). Our model makes a second read-out (Figure 5a, solid circles) once the whole stimulus evidence is fully integrated, allowing for the possibility to speed up or slow down the trajectory or even to reverse the decision. Specifically, the remaining trajectory is updated so that its vigor positively correlates with the final integrated evidence (Figure 5c). Importantly, the net impact on the vigor depends on the evidence at the second readout relative to the first readout: when the evidence is larger at the second readout, the trajectory is accelerated, whereas when it is smaller is slowed down. When the second read-out is strongly at odds with the initial targeted port, a new ballistic trajectory is drawn towards the opposite port representing a change-of-mind (Figure 5a, bottom, yellow trace). The amount of contradictory evidence necessary to reverse the trajectory is parametrized by the CoM boundary θ_{CoM} (Figure 5a).

Fitting such a complex dynamical model to experimental data is challenging because its likelihood cannot be expressed analytically. To solve this problem, we used Mixed Neural Likelihood Estimate (MNLE), a recently developed method to approximate the likelihood

function of a statistical model using an artificial network (Boelts et al. 2022). In short, an artificial neural network was trained on 10 million model simulations to approximate the joint likelihood of choice, reaction time and movement time, given the model parameters and the value of the prior evidence and stimulus strength. We confirmed that the trained model provides a good approximation to the likelihood by comparing it to extensive simulations for different sets of parameters (Supp. Figures 4, 5) (see Methods).

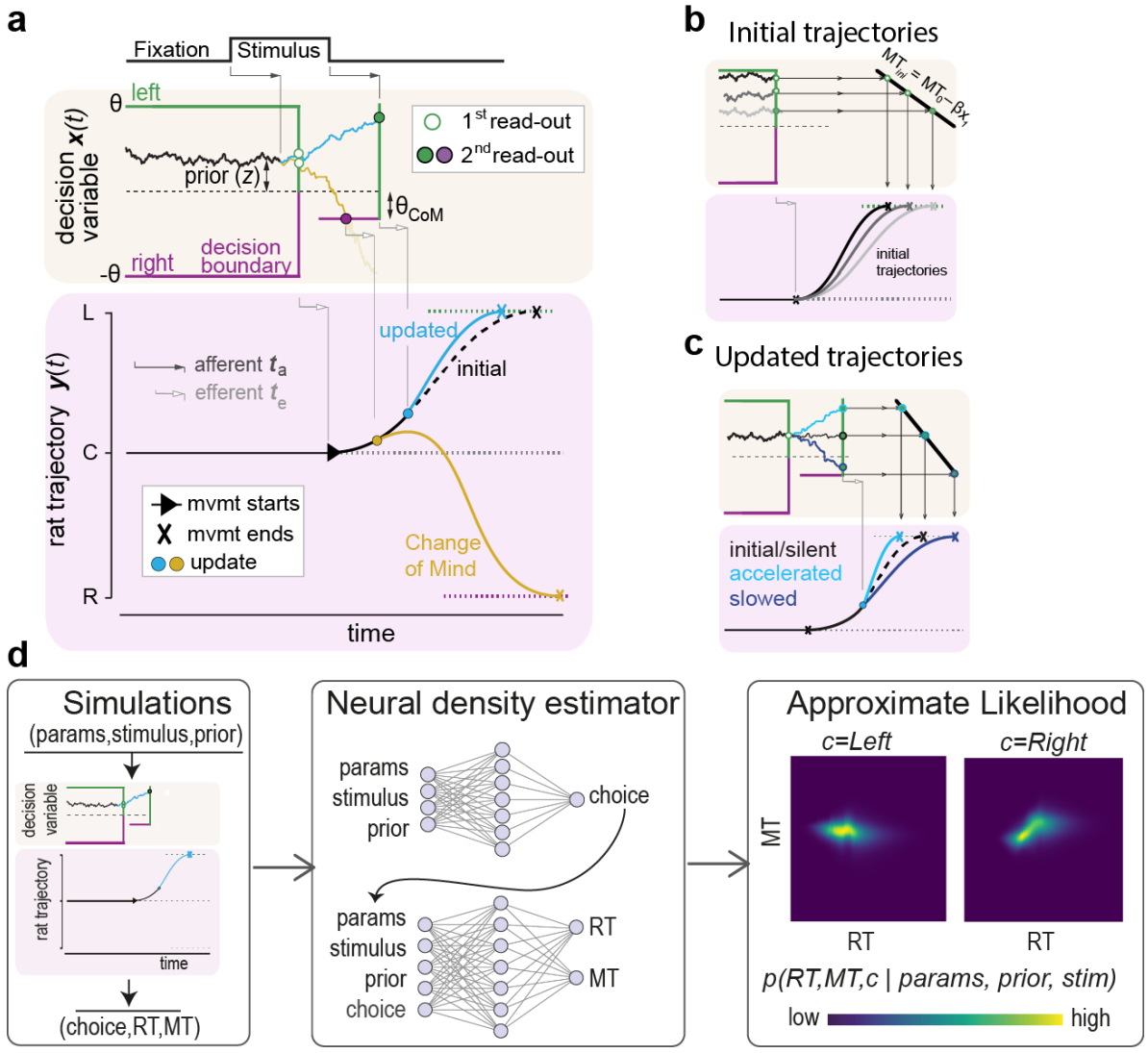

Figure 5. A joint statistical model for decision-making processes and response trajectories. **a.** The decision of the model is based on the decision variable x(t), which accumulates the sensory information towards the left (green upper bound) or right (purple lower bound) port following a drift-diffusion process. The value of x(t) at the trial onset is set by the prior evidence z (see Methods). The stimulus is integrated after a delay with respect to the stimulus onset (afferent delay, t_a, gray solid arrows). Two example trials are shown in which the movement onset is triggered by a stimulus-independent process (Hernández-Navarro et al. 2021) that sets the time of the first read-out (vertical collapse of the decision boundaries). The first readout, x_1, triggers a leftward initial trajectory (bottom panel, black trace) with an efferent delay (t_e). In the standard trial (blue trace), sensory integration continues until the stimulus is fully processed (second vertical boundary): the second

readout x_2 (solid circles) updates the vigor of the trajectory by accelerating the movement (blue trajectory). Alternatively, the stimulus may contradict the evidence set by the prior (yellow trace), driving the decision variable into the change-of-mind bound ($\boldsymbol{\theta}_{\text{CoM}}$, filled purple circle) and triggering a reversal of the trajectory (yellow trajectory). **b.** The movement time of the initial trajectory MT_{ini} depends linearly on the absolute value of x_1, where larger evidence converts into larger initial vigor. **c.** The movement time is updated by a linear transformation of the second read-out: the trajectory is sped up if $x_2 > x_1$, and slowed down otherwise. **d.** Model parameter estimation using Mixed Neural Likelihood Estimate. The model is simulated on 10 million trials, each with a different set of parameters and experimental conditions (stimulus and prior). Model simulations are then used to train an artificial neural network to approximate the conditional density of the data (i.e. choice, reaction time and movement time) given the model parameters and experimental conditions. Specifically, we train two different networks, that respectively learn $p(choice|parameters, prior, stimulus)$ and $p(RT, MT|choice, parameters, prior, stimulus)$. Finally, we estimate model parameters from experimental data using classical maximum likelihood estimation, but where the true (intractable) likelihood is replaced by the approximate likelihood provided by the trained network.

The model captured very well the impact of the prior and stimulus evidence on the animals' response trajectories (Figure 6; Supp. Figure 6). We fitted the 16 parameters of the model to the reaction times, movement times and final choices, for each rat individually. We then applied the same analyses used for the experimental data to the data generated from the fitted model. The model reproduced the experimental dependence of choice on prior, stimulus and RTs (Figure 6a-b) as well as the distributions of RT and MT (Supp. Figures 7 and 8). As the response vigor was determined by the value of the decision variable at both read-outs, the MT decreased when the prior and sensory evidence towards the response increased (Figure 6c-f). As in rats, model trajectories were faster compared to silent trials if the sensory evidence was congruent with the choice and slower if it was incongruent (Figure 6d). This follows directly from how the model updates the trajectories based on the relationship between the first and the second read-out: congruent stimuli tended to increase the initial evidence at the second read-out, causing acceleration, whereas incongruent stimuli tended to decrease it, causing slowing.

Because in express responses the sensory evidence influences the decision variable only at the second read-out (the stimulus information cannot impact the decision variable at the first read-out due to afferent and efferent delays), the stimulus evidence impacted the model trajectories only after a minimum delay of 50-100 ms following stimulus onset, as this delay includes afferent and efferent times ($t_a + t_e$= 34.0 ± 5.5 ms across animals; see also splitting times in Figure 6g). As in rats and humans, this delay was actually larger for very short reaction times (RT<20 ms), as such a short stimulus has a marginal impact on the decision variable.

Importantly, although the model was not fit to any property of the trajectories beyond their overall duration, it produces trajectory reversals (Figure 6h). These reversals occur in the same conditions as in the animals, i.e. when the stimulus is strongly incongruent with the prior (Figure 6i, Supp. Figure 9). Reversing trajectories incurs a certain time cost, which explains why trajectories with reversals last on average longer than standard trajectories (Figure 6j). Reversals are also more frequent at short RTs in the model (Figure 6k). Indeed, in such trials, while the first read-out reflects only the prior information the second read-out also incorporates the sensory information, which can contradict and overcome the prior. By

contrast, at longer RTs, the stimulus contributes to both read-outs, making changes of mind less frequent. Interestingly, our model also predicts that only around a quarter of the CoMs lead to detectable trajectory reversals (CoMs represented 15.67% of the total, whereas detected reversals were 4.44%). This is because the majority of CoMs produced by the model occur early after movement onset, yielding kinks in the trajectories that are too small to be detected. Overall, there is a compelling fit between our model and the experimental data, in terms of movement time, the timing of impact onto trajectories and the trajectory reversals. This alignment supports the hypothesis that the computation involved in performing the task corresponds to an accumulation process that encompasses the two relevant variables - prior and stimulus evidence- and tightly transforms accumulated evidence into motor response kinematics at two distinct time points.

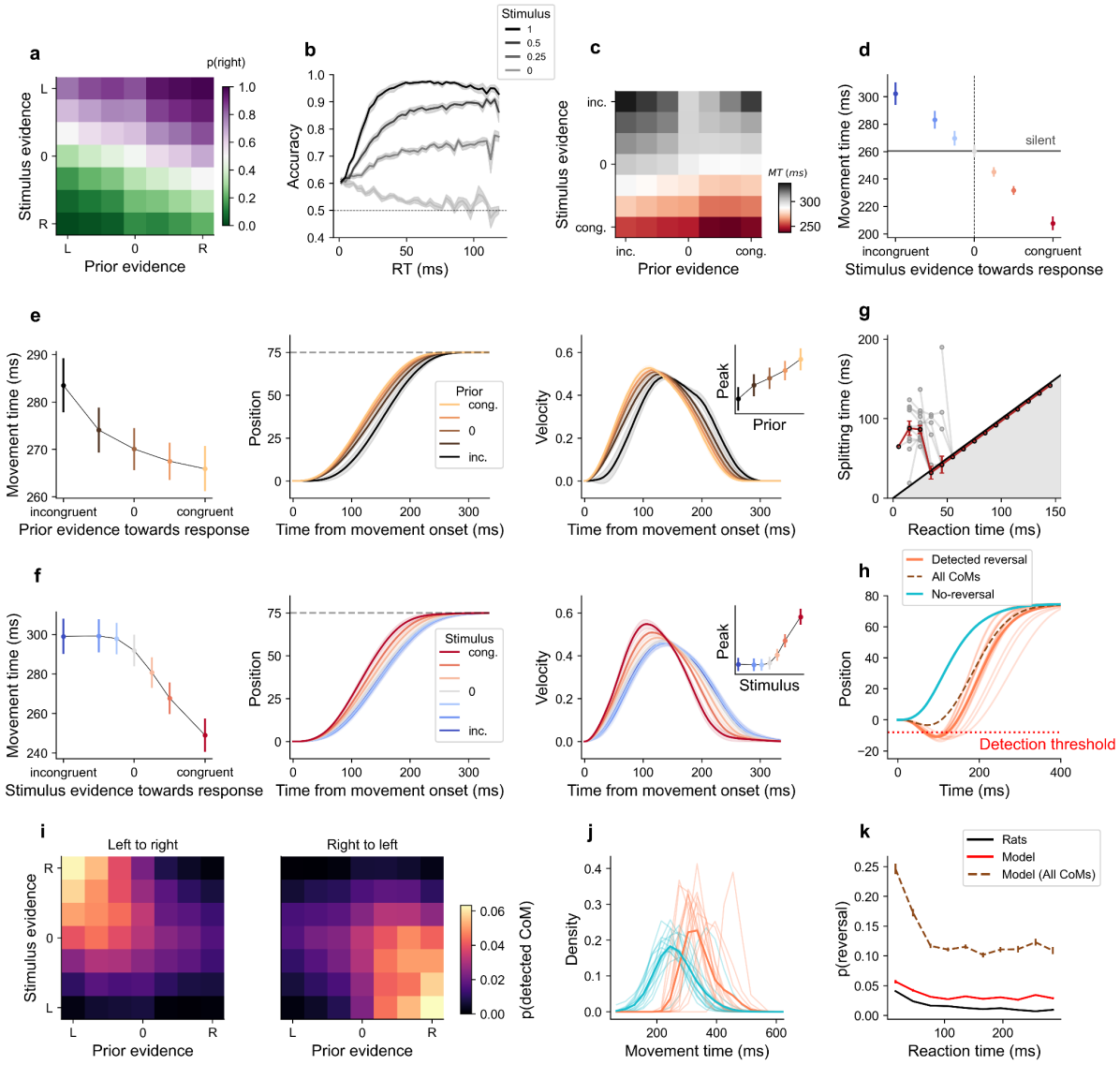

Figure 6. Simulations from the model fitted to individual rats replicate the key features of rat behavior. **a)** Proportion of right responses as a function of the stimulus and prior evidence (as in Figure 1b). **b)** Accuracy of the model as a function of RT, for different stimulus strengths (as in Figure 1d). **c)** Average movement time as a function of prior and stimulus evidence towards the selected port, averaged across animals (as in Figure 1h). **d)** Average movement time as a function of stimulus evidence supporting the decision, in express response trials (RT<50 ms) with prior evidence

supporting the decision (prior evidence towards response z > median). Congruent stimuli accelerate responses w.r.t. silent trials (dashed line), while incongruent stimuli slow down responses, as in Figure 2i. **e)** Left: Median movement time in silent trials as a function of prior evidence towards the selected port (binned in 5 quantiles), averaged across animals. Error bars: s.e.m. Model trajectories (center) and velocities (right) in silent trials depending on prior congruence (as in Figure 2d, f). **f)** Left: Median movement time in express response trials (RT< 50 ms) with small prior (|z| < 10% percentile), as a function of stimulus evidence towards the selected port. **g)** Splitting time for stimulus evidence as a function of RT, as in Figure 2i. **h)** Average simulated trajectories for CoM trajectories (brown; included detected and non-detected trajectory reversals), only detected reversals (orange line), standard trajectories (blue line). **i)** Probability of CoMs as a function of prior and stimulus evidence (see Figure 3f). j**)** Distribution of movement times for trajectories with changes of minds and standard trajectories. Legend as in Figure 3h. **k)** Proportion of trajectory reversals as a function of reaction time for rats (black trace) and simulations (red trace). Dotted line shows the proportion of model changes-of-mind.

Discussion

The advent of automatic techniques to extract the position of body parts from video footage has opened the path to rich quantitative analyses of motor behavior in freely moving animals. However these techniques had, to our knowledge, never been deployed in the context of decision-making tasks in mammals (Kane, Senne, and Scott 2023). Through rigorous analyses, we demonstrate that the response trajectories observed in rats performing a two-alternative forced choice task can be encapsulated by a dynamical model in which the motor component is steered by the evidence-accumulation process. Our model remarkably captured the dependence of trajectory reversals on stimulus, prior and reaction time, even though it was not fitted to any characteristics of the trajectory other than its overall duration. The same model successfully replicated the response trajectories described by human subjects performing an analogous task with their fingers on a tactile screen. While most previous theoretical work has focussed either on decision-making processes before a response is initiated or on the unfolding of reaching movements (Wispinski, Gallivan, and Chapman 2020), we believe that the joint modeling of decisions and response trajectories is key to dig further into the interactions between decision-making and motor control (Friedman, Brown, and Finkbeiner 2013; Lepora and Pezzulo 2015). In particular, the striking similarities between the behaviors of rats and humans suggests that rats may serve as a highly useful model for studying the neural basis of embodied decision-making. Since the motor-related activity has a large and global impact on neural activity in awake mice (Stringer et al. 2019; Musall et al. 2019), providing a foundation for models of joint decision-making and decision-related movements can significantly enhance both the analysis of neural data and our understanding of how the intertwined dynamics of decision- and motor-related activity shape cognition.

Accumulated decision evidence impacts directly and gradually motor vigor

The classical view of the brain as a serial device that orderly perceives, decides and executes its decision (Hanks and Summerfield 2017), has given way to a parallelized processing that can decide while moving and move while deciding (Gordon et al. 2021). Our work shows a direct and graded relationship between the accumulated decision evidence in a perceptual task and the vigor with which rats execute their response movements. Because

the decision variable directly tracks the subjective certainty that the selected option is correct (Bogacz et al. 2006), it follows that movement time may serve as a proxy for the internal confidence associated with perceptual decisions, just as reaction time provides similar information in fixed-duration tasks (Urai et al. 2019). To the best of our knowledge this is the first time that the vigor of a complex body movement has been tightly linked to the decision making process. Previous studies have either not found any relationship of MT with e.g. stimulus evidence (Lak et al. 2014; Zariwala et al. 2013) or have typically used paradigms that conflated both RT and MT by reporting the time from stimulus onset to movement offset), which hindered the possibility of isolating the impact of accumulated evidence on movement vigor. Saccadic eye movements (either reporting perceptual decisions or during the deliberation period, unrelated to response execution) were previously shown to be faster when perceptual evidence supporting the choice is larger (Seideman, Stanford, and Salinas 2018; Korbisch et al. 2022). Here we show that the link also exists for complex movements involving the full body, and reveal in fine detail the profound relationship between the dynamics of the decision variable and the kinematics of the movement. More broadly, because response vigor is also modulated by the intrinsic value of reward that can be obtained from these actions (Milstein and Dorris 2007; Xu-Wilson, Zee, and Shadmehr 2009; Summerside, Shadmehr, and Ahmed 2018), we can speculate that response vigor on a particular response movement is set by the expected value of that response, which depends on the probability of getting the reward that can be approximated by the decision variable.

Previous studies have identified trajectory updates in scenarios where the later part of the stimulus contradicts the earlier part (Resulaj et al. 2009; van den Berg et al. 2016) or when salient sensory evidence is contradicted by information that requires top-down processing (Nakahashi and Cisek 2023), making the subjects reverse their initial trajectory and reach the opposite option (i.e. perform a change of mind) (Resulaj et al. 2009; van den Berg et al. 2016; Nakahashi and Cisek 2023). We found that changes of mind can also occur when the stimulus violates a prior expectation, a situation that happens frequently both in naturalistic conditions (e.g. a goalkeeper during a penalty) and in the lab (e.g. the Posner task (Posner 1980)). Moreover, our results suggest that trajectory updates routinely occur even in the absence of change of final target: newly acquired sensory information leads to a slowing or speeding of the response plan. In other words, the kinematics of the motor responses are tightly linked to the dynamics of the decision process. Importantly, this adjustment of vigor is done in a graded fashion, while animals are moving towards the chosen port: rats accelerate when the newly acquired sensory information confirms their initial choice and slow down when it contradicts it. Moreover, innovative analysis of trajectories unveiled the latency of this update: the time elapsed between stimulus onset and the visible deflection of the trajectory, which encompasses a whole range of processes, from sensory processing to motor activations, can be as small as 60 ms. In humans, this minimal delay was on the order of 200 ms, which matches the minimal delay found in humans for interrupting a response movement (Schultze-Kraft et al. 2016); and is much larger than the 30 ms period required for minimal sensory integration (Stanford et al. 2010) which makes up for only one link of this sensorimotor chain.

Statistical modeling of response trajectories

Decision making tasks have been extensively characterized using computational accumulation-to-bound models such as the Drift-Diffusion Model (DDM) (Roger Ratcliff and McKoon 2008) which describe both the pattern of choices and reaction times (R. Ratcliff 1985; Palmer, Huk, and Shadlen 2005; Bogacz et al. 2010; Pardo-Vazquez et al. 2019). However, these models do not capture the impact of the decision-making process on the motor trajectories (but see (Kiani, Corthell, and Shadlen 2014)). Here we show that there is a great potential for understanding the link between decision-making and motor processes by extending the quantitative toolkit of decision processes to model response trajectories. In particular, our model can explain the main features observed in the behavior of the rats, linking the latent decision-making process with the full orienting behavior. Although the actual response involves the coordination of many effectors to reach the selected port, we found that the trajectories of the rat snout were usually smooth and stereotypical, making them amenable to standard statistical modeling. Crucially, the link between the decision and motor processes is maintained during motor execution, allowing for the update of the response trajectory using the information gathered by the decision-making module at the second readout.

The model makes several predictions for further experiments. First, it predicts that our subjects perform many more changes of mind than what is apparent from identifying trajectory reversals. These latent changes of mind could be detected by “neural reversals”, i.e. changes in the sign of the decision variable driven by sensory evidence that occur before the subject has started moving and that correlate with changes in the stimulus evidence, as observed in rats (Boyd-Meredith et al. 2022) and monkeys (Kiani et al. 2014; Kaufman et al. 2015; Peixoto et al. 2021). Second, our model includes only one extra read-out of the decision variable after the movement is initiated to correct or adjust the response. This key component of our model explains why subjects initiated the response immediately after stimulus onset and before there was time to process the stimulus (i.e. express response) but ultimately incorporated the stimulus evidence into the final decision. That way, subjects circumvent the hardwired latencies associated to the stimulus processing by leaving early and updating en route, something that not only allowed reversing the trajectory but also updating the response vigor. This is very different from the study by Resulaj and colleagues which focused on the effects of the “processing pipeline” on decisions (Resulaj et al. 2009): in particular, in their model, initial responses are always triggered when the evidence accumulation reaches a bound and subjects reversed their trajectories if the stimulus information still in the processing pipeline at the onset of this initial response contradicts it. One open question is whether more updates, or even a continuous updating, could occur along the trajectory (Friedman, Brown, and Finkbeiner 2013; Lepora and Pezzulo 2015). Consistent with previous work in humans (Friedman, Brown, and Finkbeiner 2013), our model proposes that the motor system can readout at discrete moments the relevant decision variables to adjust the ongoing movement, and that the actions occurring between readouts are ballistic submovements conveniently concatenated to minimize sharp changes in velocity . This setting is different from a continuous transformation between decision variables and movement ((Friedman, Brown, and Finkbeiner 2013; Lepora and Pezzulo 2015). The implementation of such a continuous model, would require accommodating the dynamics of evidence accumulation, which in general exhibit fast sudden changes in the decision variable, to the constraints of optimal motor control which imposes smooth, gradual

changes in velocities and acceleration. Our discrete-updating model may be an intermediate solution by which trajectories are constrained by the movement kinematics but closely tracks the evolution of decision variables across time. Finally, in navigation tasks, rats often pause, look back and forth before deciding which arm of a maze to select (Redish 2016). Such pauses were not observed in our auditory discrimination task, in which rats seemed to effortlessly incorporate new evidence into their approaching motor action.

Previous work in humans has found that trial history effects in perceptual decisions can be mediated by a bias in the drift of the accumulated evidence (Urai et al. 2019). We however modeled the influence of prior evidence purely as an offset in the initial value of the decision variable (Fig. 5a). This choice was based on the observation that the impact of prior on rat choices and vigor was strong for express responses (Figs. 1d-e and 2d,f) and decreased with RT (Supp. Fig. 1d). Moreover, the position of the rats snout during fixation already depended on the prior evidence, illustrating that the prior was impacting rats' movement even before they withdrew from the center port. The difference between our data and the mentioned study may be due to a different origin of the trial history effects: whereas in our task these history effects are adaptive to the statistics of the task, (Urai et al. 2019). The model did not incorporate idiosyncratic asymmetries in the integration of prior and stimulus, observed in some rats and humans, that resulted in asymmetric reversal probabilities (see Supp. Figure 2 and Figure 4l, respectively). Introducing fixed biases within the prior evidence as well as in the evidence accumulation drift could possibly account for these individual preferences. Another aspect that our model ignores is the reciprocal effect that motor kinematics can have on the decision making process. In other words, although we have shown the impact of the accumulated evidence on the motor trajectories, conversely the motor components may very well impact the decision (Cos, Bélanger, and Cisek 2011; Lepora and Pezzulo 2015; Shadmehr, Huang, and Ahmed 2016), a phenomenon known as embodied decision-making. For example, as the rat gets closer to one port, the weight of evidence contradicting the decision made may decrease or the boundary for changes of mind could increase, in order to avoid a reversal, which at this point would be costly.. Such a phenomenon is closely related to confirmation bias by which subjects discard evidence contradicting an initial choice (Nickerson 1998). Note however that the boundary for changes of mind was close to null in most animals (Supp Fig 10), unlike in humans (Resulaj et al. 2009), indicating a lack of bias to confirm their response even as they already departed towards the associated port.

Making decisions in a continuous world

The similarity between the behavior of rats and humans in our task suggests that the strategy used by both species to adjust movements endpoints and vigor while processing asynchronous information evolved before the two species diverged around 75 million years ago (Striedter and Glenn Northcutt 2019). Our results also suggest that these same mechanisms control very different types of motor response, such as the full-body orientation or the sliding of the finger. Consistent with this hypothesis, the basal ganglia, which regulates motor vigor (Turner and Desmurget 2010), is a highly preserved area since its emergence in the first vertebrates 500 million years ago (Grillner and Robertson 2016). This conservation may reflect the fact that embodied decisions, in which the subject acts while deciding and decides while acting (Gordon et al. 2021), have been fundamental throughout the evolutionary history of vertebrates. Future research should investigate the exact contribution

of the basal ganglia to adjusting motor vigor based on the ongoing process of evidence accumulation and decision making, and the similarities and differences across vertebrates.

Beyond their similarities, an important difference between the behavior observed in humans and rats is that the former performed many more trajectory reversals. Part of this difference is likely due simply to a greater sensitivity of our analyses to detect reversals in a finger sliding along a tablet screen than in rats moving from one port to another. However, it is also worth noting that the energetic cost of a change of trajectory is much smaller when performing a movement with a finger than with the full body. Indeed, many of the reversals done by human subjects occurred even when the finger was already close to the target port initially selected. In the future it will be important to further explore the conditions that generally determine the rate of reversals in more general conditions, in which the time-varying stream of sensory information can continue throughout the movement execution.

Methods

Rat Behavioral protocol

15 male Long-Evans rats performed a free reaction time (RT) two-alternative forced choice (2AFC) intensity discrimination task (Pardo-Vazquez et al. 2019). We summarize the structure of the task below, for further details see (Hermoso-Mendizabal et al. 2020b; Hernández-Navarro et al. 2021). Rats initiated a trial by maintaining fixation at the center port during 300 ms. A broadband noise stimulus was then presented at two speakers, and lasted until they retracted from the port and initiated a response. The relative stimulus strength (i.e. the average difference in sound intensity between the two speakers) changed every trial between different values: 0 (mean equal intensity), 0.25, 0.5 and 1 (stimulus on the correct side only). This resulted in 7 values of stimulus evidence (i.e. stimulus strength signed by the stimulus category), ranging from -1 (clear evidence to the left) to +1 (clear evidence to the right). The interaural difference fluctuated dynamically within each stimulus along the predetermined mean. Correct responses were rewarded with 25 µl of water and incorrect ones punished with 2s timeout. The stimulus category (left vs right dominant) was drawn based on the current block: in repeating blocks, the stimulus category was repeated with probability P_{rep}=0.8 (and alternated in the remaining 20%); in alternating blocks, the stimulus category was repeated with probability P_{rep}= 0.2 (and alternated in the remaining 80%). In 6 out of 15 rats we also introduced a small fraction (mean±SD 6.7 ± 0.6% of all trials) of silent trials (i.e. trials with no stimulus; see Table 1). Trials with reaction times above 400 ms or motor time above 1000 ms were excluded.

Animal groups	**# rats**	**# sessions (mean±std)**	**# trials per rat (mean ± std)**	**# Silent trials per rat (mean ± std)**
Group #1 (ILD task): LE40, LE84, LE41, LE85, LE37, LE36, LE38, LE39, LE86	9	131 ± 45	59,870 ± 25,933	0
Group #2 (ILD task + silent	6	283 ± 45	123,983	8,411

trials): LE42, LE43, LE44, LE45, LE46, LE47			± 26581	± 2,352
TOTAL	15	2,889	1,282,733	50,468

Table 1. Rat groups.

Model of prior evidence

We defined the prior evidence as the magnitude of the choice bias caused by the recent history of trials. As we described in detail in a previous work (Hermoso-Mendizabal et al. 2020a), rats leverage the trial sequence statistics to develop a prior expectation on the next rewarded side. Because history-dependent biases disappeared following an error (i.e. the prior did not guide the decision) (Hermoso-Mendizabal et al. 2020a), in the remainder of the analyses we only analyzed trials following correct responses. This prior expectation can be recapitulated by using a Generalized Linear Model of choices which quantifies the weight of different elements of recent history on choices (Busse et al. 2011; Frund, Wichmann, and Macke 2014; Abrahamyan et al. 2016; Braun, Urai, and Donner 2018; Hermoso-Mendizabal et al. 2020a). In rats, we used the same logistic regression model as in (Molano-Mazón et al. 2023) - see the reference for full model description. The model regressors include the impact of previous response repetitions/alternations (with different weights depending on whether each of the responses in the transition were rewarded) and previous rewarded and non-rewarded responses occurring in the last 10 trials. The model also includes a regressor for current stimulus S_t (defined as the average intensity difference between the two tone sounds) and a fixed side bias $\boldsymbol{\beta}_0$. After fitting the GLM model to the choices of each individual animal, the prior evidence was defined in each trial as the sum of the trial-history regressors weighted by their corresponding regression weight. For humans, due to the lower number of trials, we used an exponential kernel as a basis function for the impact of the different history regressors, as in previous studies (Frund, Wichmann, and Macke 2014) (Supp. Figure 3).

Automatic tracking of rat position

A USB camera OV2710 CMOS (3.6mm lens, 30 to 120 frames per second, 640 x 480 pixels per frame) was placed at approximately 30 cm from the floor level, recording the animal movements from above. The camera had no infra-red filter, so the rats could be recorded without being disturbed by visible light. Snout coordinates in the horizontal plane were extracted from videos using DeepLabCut (v1.11 using a resnet50 architecture) (Mathis et al. 2018). A total of 480 images from several subjects were manually labeled. 95% of the images were used to train the model, while the remaining 5% was used to evaluate its performance. The deviation (RMSE) from the snout tracking done by the model and the ground truth (human-labeled images) was 3.71 pixels for the test set (1.04 pixels for the training set).

Preprocessing of the trajectories

The output of this processing pipeline was a time-series for the coordinates of the animal snout in two dimensions *(x,y).* To compensate for small camera movements across sessions, pixel space was re-referenced on every session such that the central port was located at *y=0*

and lateral ports at coordinates *y=-75* and *y=75*- all units are expressed in pixels. The time-series were interpolated linearly to infer trajectories at a time resolution of 1 ms. All trajectories were re-referenced temporally to motion onset (*t=0*), i.e. the time at which the animal left the central port as captured by the laser. We excluded all trajectories for which the detected *y* position was above +100 pixels or below -100 pixels at any time during the reaching trajectory (1.12 % of trajectories), or when the end point of the trajectory was inconsistent with the registered response port (0.41%). On each trial, we shifted all coordinates along the y-coordinates so that *y*=0 corresponds to the average position of the animal in the last 100 ms before motor onset.

Average trajectories

We performed average trajectories and velocities for different values of the stimulus and prior evidence. To compute this, we first flipped the sign of trajectories ending at the right port so that all trajectories end around +75 pixels. We assumed that the coordinates of the snout stayed constant after reaching the response port, and padded the coordinates accordingly. The stimulus evidence towards the response corresponds to the stimulus strength (between 0 and 1) signed by the congruence with the final response. For example, if the stimulus category is rightward but the selected port is leftward, the stimulus is incongruent with the response, and so the stimulus evidence towards the response is negative. The prior evidence towards the response is defined similarly. The signed prior were binned into 5 quantiles. Instantaneous *y* velocities were computed by finite differences, i.e. they corresponded to the difference of *y* coordinates in successive frames divided by the time resolution.

Movement time analysis

Movement time was defined as the duration between the motion onset and motion offset, both registered by lasers at the corresponding ports. We measured the raw impact of prior evidence on MT by focussing on silent trials, to avoid the confound of sensory evidence. We measured the raw impact of stimulus evidence on MT by focussing on trial with small prior (|z|<10% percentile), to reduce the confound of prior evidence; and on express responses (RT<50 ms), to reduce the possible confound of reaction times (in express responses, RTs are independent of stimulus evidence). Finally, to test whether sensory evidence can speed up and/or slow down trajectories, we focussed our analysis on trials whereby the prior strongly supported the decision (prior evidence towards response z > median) in order to minimize the impact of change of trajectories; and in express response trials, to reduce the impact of RT. We also performed a linear regression analysis for MT in each animal separately, using three different regressors: the stimulus strength and the prior evidence, both signed by their congruence with the final responses (as described above); and the index of the trial within the session, an indicator of the animal satiety and fatigue (Hernández-Navarro et al. 2021). All regressors were z-scored.

Splitting time

To estimate the time at which stimulus information impacted the trajectories, we computed the splitting time of trajectories associated with different stimulus strengths. Here, we first flipped the sign of the *y* coordinates when the stimulus category was associated with the rightward responses (independently from the actual response), so that positive *y* values correspond to trajectories towards the correct port. For each time point, we computed the Pearson correlation across trials between the position of the animal along the *y* axis and the

stimulus strength. We extracted the time-series of p-value for these correlations and identified the splitting time as the last non-significant time point using a criterion of p=0.05. This analysis was performed for each animal, separately for different bins of reaction times (bin size=10 ms). The same analysis was repeated using the prior evidence instead of the stimulus evidence.

Trajectory reversals

For each trial, we measured the maximal position of the animal (along the *y* axis) in the direction contrary to the response port and labeled this as the deflection point. Trials were labeled as reversal trials if this value exceeded a certain threshold (8 pixels). We applied this thresholding to avoid spurious detections due to spontaneous movements done by the rats unrelated to the task.

Statistical model of decision-making and response trajectories

The generative model is composed of two modules: a decision-making module, which integrates the stimulus evidence and selects the response based on the accumulated evidence at the moment the response is initiated, and a motor module that translates the decisions into a reaching trajectories towards the associated port. The overall objective of the model is to jointly maximize the probability for correct choices and minimize movement costs (Rigoux and Guigon 2012; Lepora and Pezzulo 2015).

The decision-making module is based on the architecture of the Parallel Sensory Integration and Action Model (PSIAM) (Hernández-Navarro et al. 2021). In the PSIAM, a response is initiated wherever either of two parallel processes reaches a boundary: an Evidence Accumulation process that integrates decision evidence over time, akin to the Drift Diffusion Model (Roger Ratcliff and McKoon 2008); and an Action Initiation process that can trigger the initiation of the response independently of the decision evidence integration (a “go” signal that varies randomly from trial to trial). The Evidence Accumulation process represents the relative evidence in favor of each choice (or decision variable, x), with positive and negative values supporting the leftward and rightward choices, respectively. Its initial value (at fixation onset) is set proportional to the prior evidence ***z***. The dynamics of the decision variable is subject to diffusion noise $\eta(t)$ and leak λ, and integrates the stimulus evidence ***s(t)*** with drift a_P and a delay (afferent time t_a) as $dx/dt = -\lambda x + a_p s(t - t_a) + \eta(t)$. If the decision variable reaches one of two symmetric bounds ± $\boldsymbol{\theta}$, the model selects the corresponding response (first read-out) and the trajectory towards the selected port is initiated with a certain delay (efferent time t_e). A response can be also initiated if the Action Initiation process reaches its associated boundary. In that case the side of the response is determined by the sign of the decision variable at that time x_{RO1} (1st read-out). In either case, evidence integration continues after this first read-out and until the stimulus is fully integrated (i.e. with a delay of t_e+t_a with respect to the first read-out; second read-out). If during this interval the decision variable hits the boundary for changes of mind (set at a value θ_{COM} with the sign opposite to the initial response), then the initial response is reversed. Otherwise, the trajectory is confirmed and the second read-out (of value x_{RO2}) only modulates the trajectory towards the response port (see below).

The motor module translates the decisions onto motor trajectories. The initial trajectory is computed by first selecting the planned Movement Time, which depends linearly on the

evidence accumulated at the first read-out and the trial index: $MT_{ini} = \beta_0 - \beta_{DV}|x_{RO1}| + \beta_{TI}TrialIndex + \eta$ where η is drawn from a 0-centered Gumbel distribution of variance σ^2_{MT} (this distribution was used to produce right-skewed MT distribution as observed in animals, see Figure 3h). This planned MT is then converted into a full trajectory by applying the principles of minimal jerk (Flash and Hogan 1985), which is known to produce good approximations to ballistic movements. The principle specifies the full trajectory *y(t)* between a starting point y_0 and an endpoint y_E given the movement duration (or MT), and the velocity and acceleration at the start point and endpoint. This trajectory minimizes the overall jerk, that is the integral of the square of the third-order derivative of position over the entire interval. The solution is given by a 5th order polynomial: $y(t) = a_0 + a_1 t + a_2 t^2 + a_3 t^3 + a_4 t^4 + a_5 t^5$ (Shadmehr and Wise 2004). The vector of coefficients a is found by solving a linear system specifying the boundary conditions on $y(t)$, dy/dt and d^2y/dt^2 at the initial and final points t_0 and t_E:

$$M(t_0, t_E).a = b$$

where

$$M(t_0, t_e) = \begin{pmatrix} 1 & t_0 & t_0^2 & t_0^3 & t_0^4 & t_0^5 \\ 0 & 1 & 2t_0^2 & 3t_0^2 & 4t_0^3 & 5t_0^4 \\ 0 & 0 & 2 & 6t_0 & 12t_0^2 & 20t_0^3 \\ 1 & t_e & t_e^2 & t_e^3 & t_e^4 & t_e^5 \\ 0 & 1 & 2t_e^2 & 3t_e^2 & 4t_e^3 & 5t_e^4 \\ 0 & 0 & 2 & 6t_e & 12t_e^2 & 20t_e^3 \end{pmatrix}$$

and the vector b is determined by the boundary conditions $b = [y(t_0), dy/dt(t_0), d^2y/dt^2(t_0), y(t_E), dy/dt(t_E), d^2y/dt^2(t_E)]^T = [0, 0, 0, \pm 75, 0\ 0]^T$. Note that we assume null velocity and acceleration along the y-axis at the initial and ending point (the sign of the position at t_E depends on the selected response port).

Inverting this system gives $a = M(t_0, t_E)^{-1} b$.

Imposing $t_o = 0$,

$$M(t_0 = 0, t_e)^{-1} = \begin{pmatrix} 1 & 0 & 0 & 0 & 0 & 0 \\ 0 & 1 & 0 & 0 & 0 & 0 \\ 0 & 0 & \frac{1}{2} & 0 & 0 & 0 \\ -\frac{10}{t_e^3} & -\frac{6}{t_e^2} & -\frac{3}{2t_e} & \frac{10}{t_e^3} & -\frac{4}{t_e^2} & \frac{1}{2t_e} \\ \frac{15}{t_e^4} & \frac{8}{t_e^3} & \frac{3}{2t_e^2} & -\frac{15}{t_e^4} & \frac{7}{t_e^3} & \frac{-1}{t_e^2} \\ -\frac{6}{t_e^5} & -\frac{3}{t_e^4} & -\frac{1}{2t_e^3} & \frac{6}{t_e^5} & -\frac{3}{t_e^4} & \frac{1}{2t_e^3} \end{pmatrix}$$

The initial trajectory is later updated following the second read-out at time $t_U = t_{RO2} + t_e$. If that second read-out leads to a change of mind, the endpoint is changed to the alternative response port (Friedman, Brown, and Finkbeiner 2013). If no change of mind is produced,

the response port stays unchanged but the end time is updated. In all cases, the endtime changes according to $t'_E = t_E - \beta_U |x_{RO2} - x_{RO1}|$. In other words, the trajectory is sped up w.r.t the original trajectory if the decision variable at the second read-out is larger in amplitude than at the first read-out, and is slowed down otherwise. The updated trajectory between t_U and t_E is drawn again using the minimum-jerk principle, solving a new linear equation as seen above but where the initial conditions correspond to the position, velocity and acceleration of the initial trajectory at time t_U (due to the continuity of these variables).

The model contains 18 parameters overall: 5 parameters related to the Action Initiation process (t_{AI}, v_{AI}, w_{AI}, σ^2_{AI}, θ_{AI}), 8 parameters to the Evidence Accumulation process, (t_A, t_E, z_P, v, λ, σ^2_{DV}, θ_{DV}, θ_{COM}) and 5 parameters to the response trajectories (β_o, σ^2_{MT}, β_{DV}, β_{TI}, β_U). Parameters σ^2_{AI} and σ^2_{DV} were set to one to avoid identifiability issues for the AI and DV process. Model simulations produced trajectories that we sampled at a 1000-Hz rate.

Model fitting

The model parameters were fitted to the joint pattern of choices, reaction times and movement times, separately for each rat. Because the likelihood of such a model cannot be expressed analytically, we used Mixed Neural Likelihood Estimator (MNLE), a simulation-based method to approximate the likelihood of a model designed for mixed data (e.g. RT and choice), as typically found in decision-making tasks (Boelts et al. 2022). Here, the mixed data corresponds to one binary variable (choice) and two continuous variables (RT and MT). MNLE consists of training an artificial neural network that takes model parameters as input and outputs a joint probability distribution for the dependent variable. We extended the method to also include per-trial conditions (stimulus evidence s_t, prior evidence z_t, trial index ti_t) as extra input to the network. Thus the model approximated $p(c, RT, MT|\theta, s_t, z_t, ti_t)$. More precisely, the method relies on training two separate networks, one that learns the conditional probability $p(c|\theta, s_t, z_t, ti_t)$, while the other learns the conditional density $p(RT, MT|c, \theta, s_t, z_t, ti_t)$. The network was trained on 10 million simulations on the model: in each simulation, the model parameters were sampled from uniform distributions over plausible values, while the per-trial conditions corresponded to one trial randomly selected from the experimental dataset. For additional details about the model architecture and training, refer to the original publication (Boelts et al. 2022). Finally, we checked that the likelihood approximation improves as the training set size increased (Supp. Figure 5g-h).

We checked that the trained network provided a good approximation to the true likelihood in three different ways. First, we compared its output for a fixed parameter set to the density obtained from 500.000 model simulations at the same parameter values (Supp. Figure 4). This was repeated for a set of 6 trial examples covering all prototypes of prior-stimulus association and different levels of trial index. Second, we checked the robustness of the method by comparing the approximated likelihood of two networks trained with two different sets of 10 million simulations (Supp. Figure 5 a-f). Finally, we confirmed that the likelihood

approximation improves as the size of the training set increases (Supp. Figure 5). We then fitted the model for each individual rat through maximum likelihood estimation, where the true likelihood was based on the approximate likelihood provided by the trained network. To limit the impact of possible outliers on parameter estimation, we used a mixture of two distributions, the approximated distribution and a contaminant distribution: $p(c, RT, MT|\theta, s_t, z_t, ti_t) = (1 - \varepsilon)p_{MNLE}(c, RT, MT|\theta, s_t, z_t, ti_t) + \varepsilon p_C(c, RT, MT)$. The contaminant was simply set as a uniform distribution (with RT bounded between 0 and RT_{max}=1, and MT bounded between 0 and MT_{max}=0.4), i.e. $p_C(c, RT, MT) = 1/(2RT_{max}MT_{max})$. The mixture parameter ε was set to 10^{-3}. Because fixation breaks (i.e RT<0) have no associated choice nor movement time (the trial was aborted), we replaced the joint likelihood term for these trials by the likelihood of the reaction time, i.e. we defined the overall likelihood as $L(\theta) = \sum_{RT_t>0} log\, p(c_t, RT_t, MT_t|\theta, s_t, z_t, ti_t) + \sum_{RT_t<0} log\, p(RT_t|\theta, s_t, z_t, ti_t)$. The likelihood of the reaction time alone can be expressed analytically as the RT distribution in negative trials (which corresponds only to AI-triggered responses) follows an inverse Gaussian distribution (Hernández-Navarro et al. 2021). The optimization procedure relied on Bayesian adaptive direct search (BADS) (Acerbi and Ma, 2017), implemented in the PyBads package.

Human behavioral paradigm

We tested *n*=20 volunteer participants (10 females and 10 males, 19 right-handed and 1 left-handed, age 19-26) performing a task that mimicked the rodent task. The task was performed on an iPad tablet with 60 Hz frame rate at a viewing distance of 50 cm, using the StimuliApp software (Marin-Campos et al. 2021). On each trial, a black screen with three gray circles appeared: the starting point, located at the bottom of the screen, at coordinates (0,-200), and the two response points, located symmetrically at coordinates (-600,400) and (600,400). Subjects initiated each trial by maintaining their index finger of their preferred hand pressed against the starting point during 500 ms. The white-noise stimulus was then presented binaurally using Sennheiser headphones. The relative interaural difference between stimulus strength changed every trial between different values: 0 (mean equal intensity), 0.1, 0.2 and 0.4; the mean intensity was constant throughout the trials. Subjects had to slide the finger towards the target point at the side corresponding to the loudest stimulus. The stimulus was interrupted as soon as the finger slid away from the starting point. Feedback was provided after reaching the target point. correct choices were indicated by the whole screen turning green during 300 ms whereas errors were signaled by a red screen. Importantly, subjects had to start moving the finger within 300 ms after stimulus onset, otherwise the trial was considered a missed trial and the screen turned yellow. This time constraint introduced an urgency component which nudged participants into relying more on prior expectations. The screen also turned to yellow if subjects initiated a response before the end of the fixation period. The trial sequence statistics replicated the task used for the rats. The probability of repeating the previous stimulus category (left/right), P_{rep}, varied between Repeating blocks (P_{rep}=0.8) and Alternating blocks (P_{rep}=0.2). Blocks changed every 80 trials, without noticing the participant. Subjects were not informed about this correlation structure. The session lasted on average 1 hour and 40 minutes (interleaved by pauses every 100 trials), yielding between 2000 ± 317 trials (mean ± std) per participant.

Subjects performed a training of 200 trials before completing the task. Subjects received monetary compensation that depended on their performance (20€ + 0.01€ x N_{corr}, where N_{corr} is the number of correct responses). The study was approved by the Ethics Committee for Clinical Research of the Barcelona Clinic Hospital.

Analysis of human experimental data

We discarded three subjects that performed the task close to chance level (61.1%, 68.5% and 62.9%). We discarded another four participants who displayed a strategy to move their finger vertically first without targeting any of the two response ports, and then changed their trajectory towards one of the ports based on the stimulus (Chapman et al. 2010; Haith, Huberdeau, and Krakauer 2015). Fixation breaks and late response were excluded from the analyses. We grouped all the trials from the remaining subjects together (except for the analysis of splitting time which was performed separately for each subject). As for the rats, we analyzed only after-correct trials. This preprocess yielded a total of 24,542 trials. We analyzed the trajectories of the finger press from the starting point to the response point. Trajectories were obtained at a sample rate of 60 Hz, which were linearly interpolated to a 1000 Hz rate.

Acknowledgements

The work was supported by the Spanish State Research Agency (RYC-2017-23231 to AH and AGD, PID2019-111629GB-I00 to AH, MMM and AGD), Spanish Ministry of Economy and Competitiveness together with the European Regional Development Fund grant SAF2015-70324-R (to JR), European Research Council grant ERC-2015-CoG-683209 under the European Union's Horizon 2020 (to JR). Part of the work was developed in the Centre Esther Koplowitz (Barcelona).

References

Acerbi, & Ma. 2017. Practical Bayesian optimization for model fitting with Bayesian adaptive direct search. Advances in neural information processing systems, 30.

Abrahamyan, Arman, Laura Luz Silva, Steven C. Dakin, Matteo Carandini, and Justin L. Gardner. 2016. "Adaptable History Biases in Human Perceptual Decisions." *Proceedings of the National Academy of Sciences*. https://doi.org/10.1073/pnas.1518786113.

Berg, Ronald van den, Kavitha Anandalingam, Ariel Zylberberg, Roozbeh Kiani, Michael N. Shadlen, and Daniel M. Wolpert. 2016. "A Common Mechanism Underlies Changes of Mind about Decisions and Confidence." *eLife* 5 (February): e12192.

Boelts, Jan, Jan-Matthis Lueckmann, Richard Gao, and Jakob H. Macke. 2022. "Flexible and Efficient Simulation-Based Inference for Models of Decision-Making." *eLife* 11 (July). https://doi.org/10.7554/eLife.77220.

Bogacz, Rafal, Eric Brown, Jeff Moehlis, Philip Holmes, and Jonathan D. Cohen. 2006. "The Physics of Optimal Decision Making: A Formal Analysis of Models of Performance in Two-Alternative Forced-Choice Tasks." *Psychological Review* 113 (4): 700–765.

Bogacz, Rafal, Eric-Jan Wagenmakers, Birte U. Forstmann, and Sander Nieuwenhuis. 2010. "The Neural Basis of the Speed–accuracy Tradeoff." *Trends in Neurosciences* 33 (1): 10–16.

Boyd-Meredith, J. Tyler, Alex T. Piet, Emily Jane Dennis, Ahmed El Hady, and Carlos D. Brody. 2022. "Stable Choice Coding in Rat Frontal Orienting Fields across

Model-Predicted Changes of Mind.” *Nature Communications* 13 (1): 3235.
Braun, Anke, Anne E. Urai, and Tobias H. Donner. 2018. “Adaptive History Biases Result from Confidence-Weighted Accumulation of Past Choices.” *The Journal of Neuroscience: The Official Journal of the Society for Neuroscience* 38 (10): 2418–29.
Busse, Laura, Asli Ayaz, Neel T. Dhruv, Steffen Katzner, Aman B. Saleem, Marieke L. Schölvinck, Andrew D. Zaharia, and Matteo Carandini. 2011. “The Detection of Visual Contrast in the Behaving Mouse.” *The Journal of Neuroscience: The Official Journal of the Society for Neuroscience* 31 (31): 11351–61.
Chapman, Craig S., Jason P. Gallivan, Daniel K. Wood, Jennifer L. Milne, Jody C. Culham, and Melvyn A. Goodale. 2010. “Reaching for the Unknown: Multiple Target Encoding and Real-Time Decision-Making in a Rapid Reach Task.” *Cognition* 116 (2): 168–76.
Cos, Ignasi, Nicolas Bélanger, and Paul Cisek. 2011. “The Influence of Predicted Arm Biomechanics on Decision Making.” *Journal of Neurophysiology* 105 (6): 3022–33.
Flash, T., and N. Hogan. 1985. “The Coordination of Arm Movements: An Experimentally Confirmed Mathematical Model.” *The Journal of Neuroscience: The Official Journal of the Society for Neuroscience* 5 (7): 1688–1703.
Friedman, Jason, Scott Brown, and Matthew Finkbeiner. 2013. “Linking Cognitive and Reaching Trajectories via Intermittent Movement Control.” *Journal of Mathematical Psychology* 57 (3): 140–51.
Frund, I., F. A. Wichmann, and J. H. Macke. 2014. “Quantifying the Effect of Intertrial Dependence on Perceptual Decisions.” *Journal of Vision*. https://doi.org/10.1167/14.7.9.
Gallivan, Jason P., Craig S. Chapman, Daniel M. Wolpert, and J. Randall Flanagan. 2018. “Decision-Making in Sensorimotor Control.” *Nature Reviews. Neuroscience* 19 (9): 519–34.
Gold, Joshua I., and Michael N. Shadlen. 2007. “The Neural Basis of Decision Making.” *Annual Review of Neuroscience* 30: 535–74.
Good, I. J. 1979. “Studies in the History of Probability and Statistics. XXXVII A. M. Turing’s Statistical Work in World War II.” *Biometrika* 66 (2): 393–96.
Gordon, Jeremy, Antonella Maselli, Gian Luca Lancia, Thomas Thiery, Paul Cisek, and Giovanni Pezzulo. 2021. “The Road towards Understanding Embodied Decisions.” *Neuroscience and Biobehavioral Reviews* 131 (December): 722–36.
Grillner, Sten, and Brita Robertson. 2016. “The Basal Ganglia Over 500 Million Years.” *Current Biology: CB* 26 (20): R1088–1100.
Gupta, Diksha, Brian DePasquale, Charles D. Kopec, and Carlos D. Brody. 2023. “Trial-History Biases in Evidence Accumulation Can Give Rise to Apparent Lapses.” *bioRxiv : The Preprint Server for Biology*, February. https://doi.org/10.1101/2023.01.18.524599.
Haith, Adrian M., David M. Huberdeau, and John W. Krakauer. 2015. “Hedging Your Bets: Intermediate Movements as Optimal Behavior in the Context of an Incomplete Decision.” *PLoS Computational Biology* 11 (3): e1004171.
Hanks, Timothy D., and Christopher Summerfield. 2017. “Perceptual Decision Making in Rodents, Monkeys, and Humans.” *Neuron* 93 (1): 15–31.
Hawkins, Guy E., and Andrew Heathcote. 2021. “Racing against the Clock: Evidence-Based versus Time-Based Decisions.” *Psychological Review* 128 (2): 222–63.
Hermoso-Mendizabal, Ainhoa, Alexandre Hyafil, Pavel E. Rueda-Orozco, Santiago Jaramillo, David Robbe, and Jaime de la Rocha. 2020a. “Response Outcomes Gate the Impact of Expectations on Perceptual Decisions.” *Nature Communications* 11 (1): 1057.
———. 2020b. “Author Correction: Response Outcomes Gate the Impact of Expectations on Perceptual Decisions.” *Nature Communications* 11 (1): 3470.
Hernández-Navarro, Lluís, Ainhoa Hermoso-Mendizabal, Daniel Duque, Jaime de la Rocha, and Alexandre Hyafil. 2021. “Proactive and Reactive Accumulation-to-Bound Processes Compete during Perceptual Decisions.” *Nature Communications* 12 (1): 7148.
Kane, Gary A., Ryan A. Senne, and Benjamin B. Scott. 2023. “Rat Movements Reflect Internal Decision Dynamics in an Evidence Accumulation Task.” *bioRxiv : The Preprint Server for Biology*, September. https://doi.org/10.1101/2023.09.11.556575.

Kaufman, Matthew T., Mark M. Churchland, Stephen I. Ryu, and Krishna V. Shenoy. 2015. “Vacillation, Indecision and Hesitation in Moment-by-Moment Decoding of Monkey Motor Cortex.” *eLife* 4 (May): e04677.

Kiani, Roozbeh, Leah Corthell, and Michael N. Shadlen. 2014. “Choice Certainty Is Informed by Both Evidence and Decision Time.” *Neuron* 84 (6): 1329–42.

Kiani, Roozbeh, Christopher J. Cueva, John B. Reppas, and William T. Newsome. 2014. “Dynamics of Neural Population Responses in Prefrontal Cortex Indicate Changes of Mind on Single Trials.” *Current Biology: CB* 24 (13): 1542–47.

Korbisch, Colin C., Daniel R. Apuan, Reza Shadmehr, and Alaa A. Ahmed. 2022. “Saccade Vigor Reflects the Rise of Decision Variables during Deliberation.” *Current Biology: CB* 32 (24): 5374–81.e4.

Lak, Armin, Gil M. Costa, Erin Romberg, Alexei A. Koulakov, Zachary F. Mainen, and Adam Kepecs. 2014. “Orbitofrontal Cortex Is Required for Optimal Waiting Based on Decision Confidence.” *Neuron* 84 (1): 190–201.

Lepora, Nathan F., and Giovanni Pezzulo. 2015. “Embodied Choice: How Action Influences Perceptual Decision Making.” *PLoS Computational Biology* 11 (4): e1004110.

Mathis, Alexander, Pranav Mamidanna, Kevin M. Cury, Taiga Abe, Venkatesh N. Murthy, Mackenzie Weygandt Mathis, and Matthias Bethge. 2018. “DeepLabCut: Markerless Pose Estimation of User-Defined Body Parts with Deep Learning.” *Nature Neuroscience* 21 (9): 1281–89.

Milstein, David M., and Michael C. Dorris. 2007. “The Influence of Expected Value on Saccadic Preparation.” *The Journal of Neuroscience: The Official Journal of the Society for Neuroscience* 27 (18): 4810–18.

Molano-Mazón, Manuel, Yuxiu Shao, Daniel Duque, Guangyu Robert Yang, Srdjan Ostojic, and Jaime de la Rocha. 2023. “Recurrent Networks Endowed with Structural Priors Explain Suboptimal Animal Behavior.” *Current Biology: CB*, January. https://doi.org/10.1016/j.cub.2022.12.044.

Musall, Simon, Matthew T. Kaufman, Ashley L. Juavinett, Steven Gluf, and Anne K. Churchland. 2019. “Single-Trial Neural Dynamics Are Dominated by Richly Varied Movements.” *Nature Neuroscience* 22 (10): 1677–86.

Nakahashi, Ayuno, and Paul Cisek. 2023. “Parallel Processing of Value-Related Information during Multi-Attribute Decisions.” *Journal of Neurophysiology* 130 (4): 967–79.

Nickerson, Raymond S. 1998. “Confirmation Bias: A Ubiquitous Phenomenon in Many Guises.” *Review of General Psychology: Journal of Division 1, of the American Psychological Association* 2 (2): 175–220.

Palmer, John, Alexander C. Huk, and Michael N. Shadlen. 2005. “The Effect of Stimulus Strength on the Speed and Accuracy of a Perceptual Decision.” *Journal of Vision* 5 (5): 376–404.

Pardo-Vazquez, Jose L., Juan R. Castiñeiras-de Saa, Mafalda Valente, Iris Damião, Tiago Costa, M. Inês Vicente, André G. Mendonça, Zachary F. Mainen, and Alfonso Renart. 2019. “The Mechanistic Foundation of Weber’s Law.” *Nature Neuroscience* 22 (9): 1493–1502.

Peixoto, Diogo, Jessica R. Verhein, Roozbeh Kiani, Jonathan C. Kao, Paul Nuyujukian, Chandramouli Chandrasekaran, Julian Brown, et al. 2021. “Decoding and Perturbing Decision States in Real Time.” *Nature* 591 (7851): 604–9.

Posner, M. I. 1980. “Orienting of Attention.” *The Quarterly Journal of Experimental Psychology* 32 (1): 3–25.

Ratcliff, R. 1985. “Theoretical Interpretations of the Speed and Accuracy of Positive and Negative Responses.” *Psychological Review* 92 (2): 212–25.

Ratcliff, Roger, and Gail McKoon. 2008. “The Diffusion Decision Model: Theory and Data for Two-Choice Decision Tasks.” *Neural Computation* 20 (4): 873–922.

Redish, A. David. 2016. “Vicarious Trial and Error.” *Nature Reviews. Neuroscience* 17 (3): 147–59.

Resulaj, Arbora, Roozbeh Kiani, Daniel M. Wolpert, and Michael N. Shadlen. 2009. “Changes of Mind in Decision-Making.” *Nature* 461 (7261): 263–66.

Rigoux, Lionel, and Emmanuel Guigon. 2012. “A Model of Reward- and Effort-Based Optimal Decision Making and Motor Control.” *PLoS Computational Biology* 8 (10): e1002716.

Schultze-Kraft, Matthias, Daniel Birman, Marco Rusconi, Carsten Allefeld, Kai Görgen, Sven Dähne, Benjamin Blankertz, and John-Dylan Haynes. 2016. “The Point of No Return in Vetoing Self-Initiated Movements.” *Proceedings of the National Academy of Sciences of the United States of America* 113 (4): 1080–85.

Seideman, Joshua A., Terrence R. Stanford, and Emilio Salinas. 2018. “Saccade Metrics Reflect Decision-Making Dynamics during Urgent Choices.” *Nature Communications* 9 (1): 2907.

Shadmehr, Reza, Helen J. Huang, and Alaa A. Ahmed. 2016. “A Representation of Effort in Decision-Making and Motor Control.” *Current Biology: CB* 26 (14): 1929–34.

Shadmehr, Reza, Thomas R. Reppert, Erik M. Summerside, Tehrim Yoon, and Alaa A. Ahmed. 2019. “Movement Vigor as a Reflection of Subjective Economic Utility.” *Trends in Neurosciences* 42 (5): 323–36.

Shadmehr, Reza, and Steven P. Wise. 2004. *The Computational Neurobiology of Reaching and Pointing: A Foundation for Motor Learning*. MIT Press.

Song, Joo-Hyun, and Ken Nakayama. 2009. “Hidden Cognitive States Revealed in Choice Reaching Tasks.” *Trends in Cognitive Sciences* 13 (8): 360–66.

Stanford, Terrence R., Swetha Shankar, Dino P. Massoglia, M. Gabriela Costello, and Emilio Salinas. 2010. “Perceptual Decision Making in Less than 30 Milliseconds.” *Nature Neuroscience* 13 (3): 379–85.

Stone, Caleb, Jason B. Mattingley, and Dragan Rangelov. 2022. “On Second Thoughts: Changes of Mind in Decision-Making.” *Trends in Cognitive Sciences* 26 (5): 419–31.

Striedter, Georg F., and R. Glenn Northcutt. 2019. *Brains Through Time: A Natural History of Vertebrates*. Oxford University Press.

Stringer, Carsen, Marius Pachitariu, Nicholas Steinmetz, Charu Bai Reddy, Matteo Carandini, and Kenneth D. Harris. 2019. “Spontaneous Behaviors Drive Multidimensional, Brainwide Activity.” *Science* 364 (6437): 255.

Summerside, Erik M., Reza Shadmehr, and Alaa A. Ahmed. 2018. “Vigor of Reaching Movements: Reward Discounts the Cost of Effort.” *Journal of Neurophysiology* 119 (6): 2347–57.

Thura, David. 2020. “Decision Urgency Invigorates Movement in Humans.” *Behavioural Brain Research* 382 (March): 112477.

Thura, David, Ignasi Cos, Jessica Trung, and Paul Cisek. 2014. “Context-Dependent Urgency Influences Speed–Accuracy Trade-Offs in Decision-Making and Movement Execution.” *The Journal of Neuroscience: The Official Journal of the Society for Neuroscience* 34 (49): 16442–54.

Turner, Robert S., and Michel Desmurget. 2010. “Basal Ganglia Contributions to Motor Control: A Vigorous Tutor.” *Current Opinion in Neurobiology* 20 (6): 704–16.

Urai, Anne E., Jan Willem de Gee, Konstantinos Tsetsos, and Tobias H. Donner. 2019. “Choice History Biases Subsequent Evidence Accumulation.” *eLife* 8 (July). https://doi.org/10.7554/eLife.46331.

Wald, Abraham. 2004. *Sequential Analysis*. Courier Corporation.

Wispinski, Nathan J., Jason P. Gallivan, and Craig S. Chapman. 2020. “Models, Movements, and Minds: Bridging the Gap between Decision Making and Action.” *Annals of the New York Academy of Sciences* 1464 (1): 30–51.

Xu-Wilson, Minnan, David S. Zee, and Reza Shadmehr. 2009. “The Intrinsic Value of Visual Information Affects Saccade Velocities.” *Experimental Brain Research. Experimentelle Hirnforschung. Experimentation Cerebrale* 196 (4): 475–81.

Zariwala, Hatim A., Adam Kepecs, Naoshige Uchida, Junya Hirokawa, and Zachary F. Mainen. 2013. “The Limits of Deliberation in a Perceptual Decision Task.” *Neuron* 78 (2): 339–51.

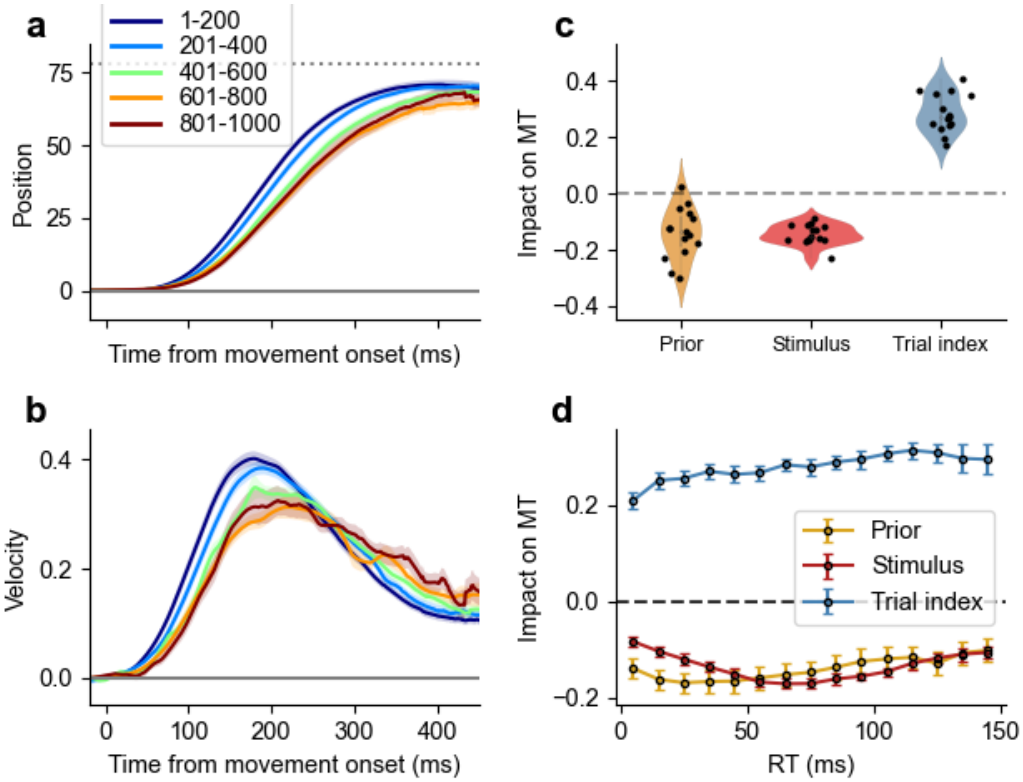

Supplementary figure 1. Trial index plays an important role for vigor. **a, b)** Average position in pixels (a) and velocity in pixels/s (b) conditioned on the trial index, grouped by bins of 200 trials. **c)** Regression weights of the movement time against prior evidence towards the response, stimulus evidence towards the response, and trial index. **d)** Regression weights of the movement time against the trial index and the prior and stimulus evidence towards the response, for different bins of reaction time. The impact of stimulus evidence is lower for very short RTs (i.e. very short stimuli) while the impact of the prior decreases with increasing reaction time. This pattern is expected for an accumulation model where the movement time depends on the readout of a decision variable whose offset and drift are determined by the prior and stimulus evidence, respectively.

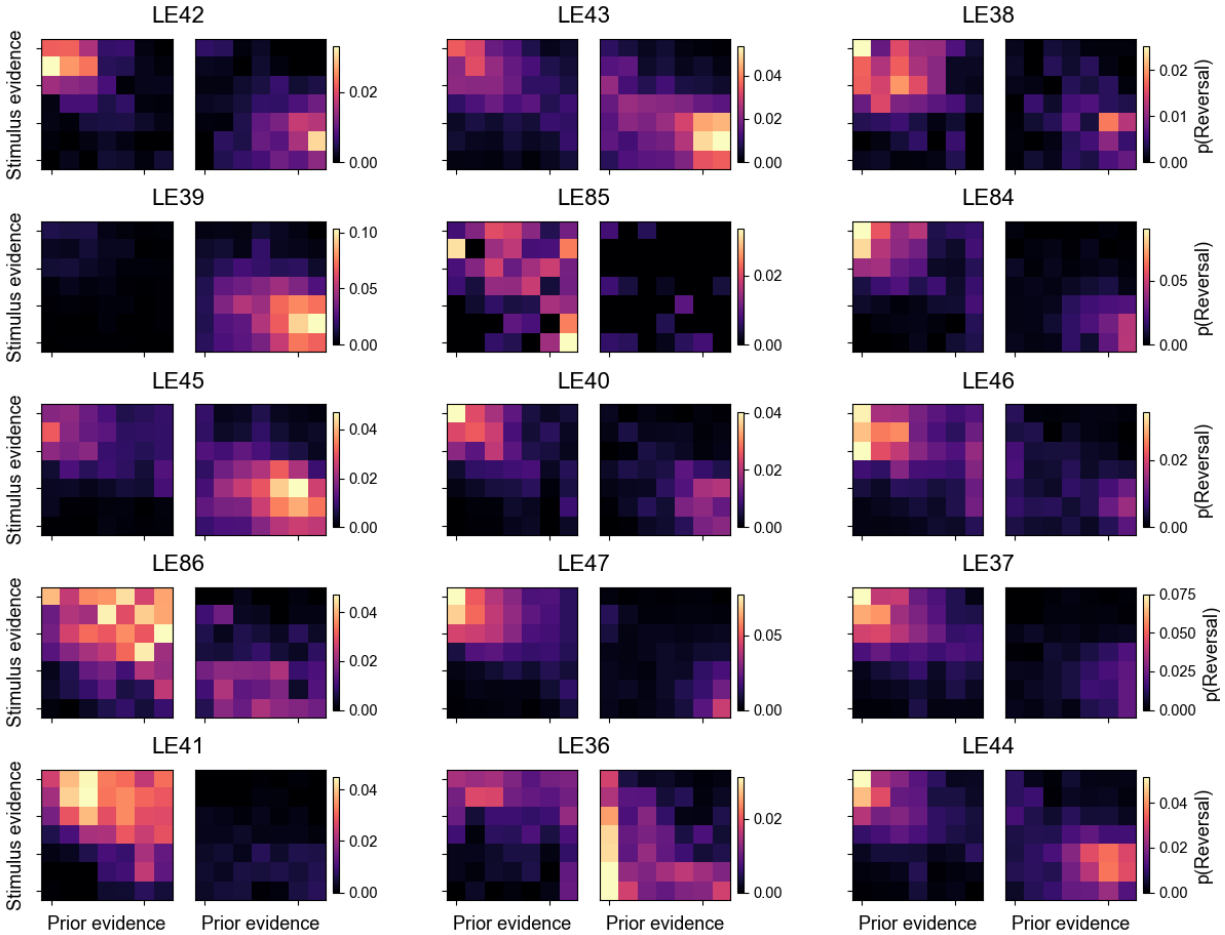

Supplementary figure 2. Proportion of left-to-right reversals (left matrices) and right-to-left reversals (right matrices) as a function of stimulus and prior evidence, rat by rat.

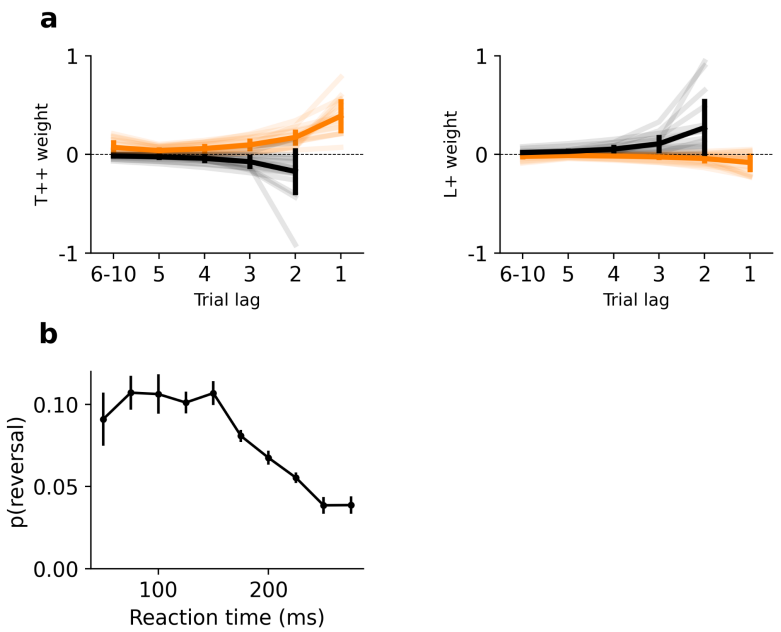

Supplementary figure 3. a) GLM transition and lateral weights for human participants. Orange: after correct trials; black: after error trials. Thin lines denote individual participants; black lines represent the

average across participants (error bars: s.e.m.). **b)** Proportion of trajectory reversals as a function of reaction time for humans.

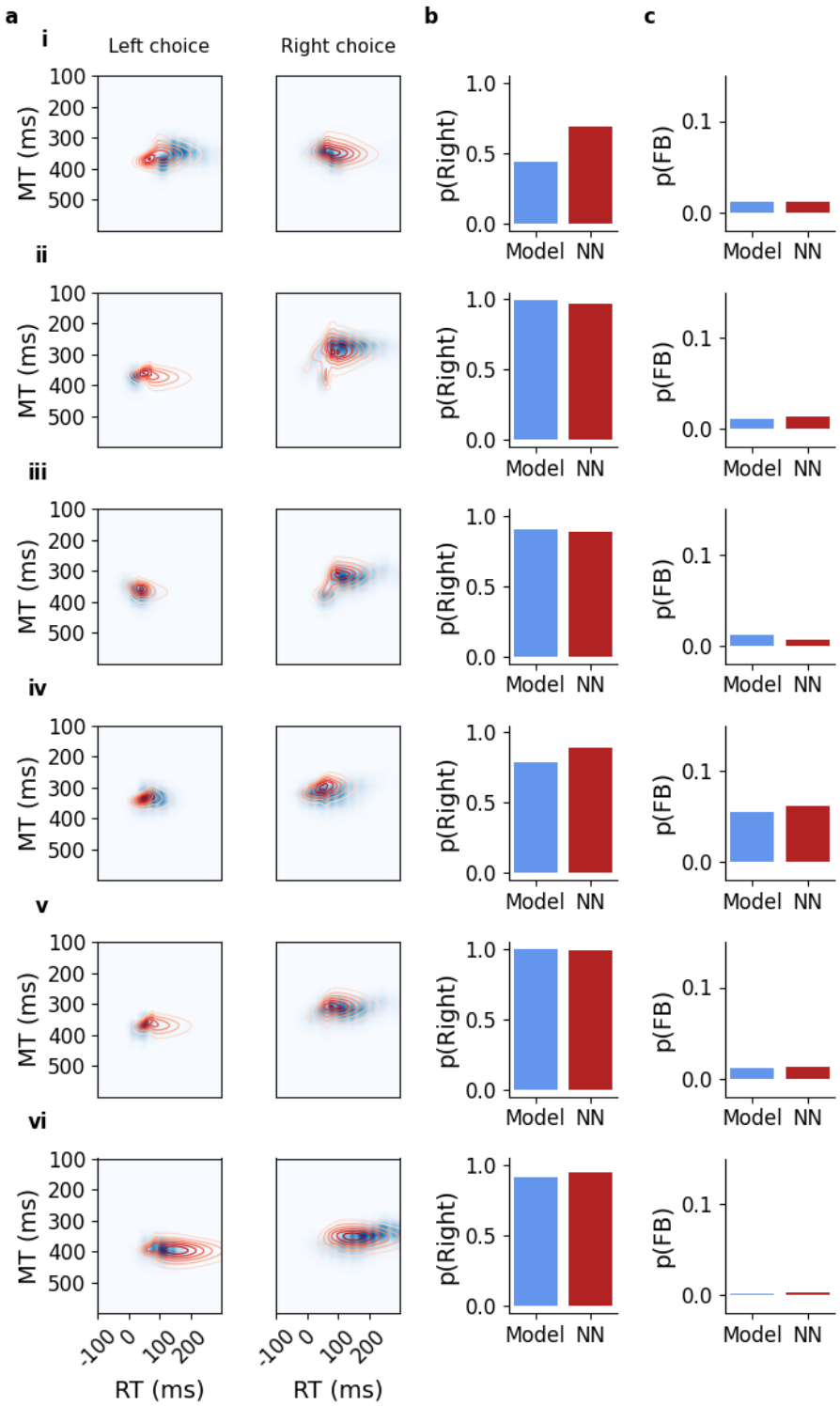

Supplementary figure 4. MNLE can approximate the likelihood of the model. Each row represents fixed trial conditions (stimulus, prior and trial index). **a)** Likelihood for the model (blue-shaded matrix) based on 0.5M simulations and approximated likelihood obtained from the MNLE trained with 10M simulations (red contours); for left and right responses, respectively. **b-c)** Probability of rightward

choice (b) and fixation break (c) for both model and MNLE. We used 6 prototypical experimental conditions: **i)** No stimulus evidence (s=0), prior towards the right (z=1.5), medium trial index (t.i.=400). **ii)** Low prior towards the right choice (z=0.05), congruent high stimulus strength (s=1), medium trial index (t.i.=400). **iii)** Incongruent prior (z=-1.5) and high stimulus (s=0.5), medium trial index (t.i.=400). **iv)** Congruent low prior (z=0.5) and low stimulus (s=0.25), low trial index (t.i.=10). **v)** Congruent and high prior (z=0.5) and stimulus (s=0.5), medium trial index (t.i.=400). **vi)** Congruent prior (z=0.5) and stimulus (s=0.25), high trial index (t.i.=800).

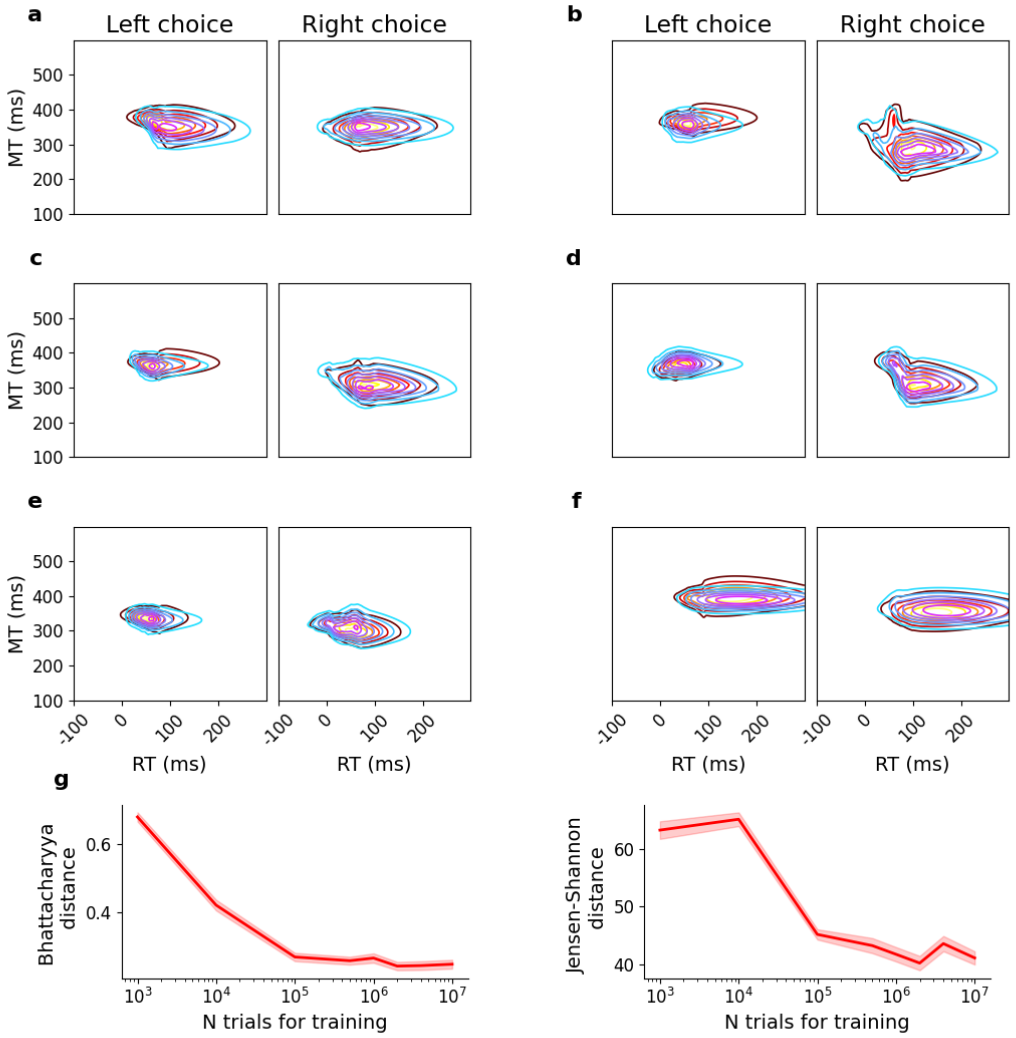

Supplementary figure 5. MNLE likelihood from two networks trained with 10M simulations. **a-f)** Same trials as in the previous figure (Supp. Figure 4). **g)** Distance between the probability distributions from the network and the model, for different sizes of training sets for the neural network. We computed two distance metrics using 200.000 model simulations for 100 random trials (Supp. Figure 5). The metrics used were the Bhattacharyya distance (left panel), defined as $d(P,\ Q)\ =\ -\ ln(\sum_i(\sqrt{P(x_i)\cdot\ Q(x_i)}))$; and the Jensen-Shannon distance

(right panel), defined as $d(P,\ Q)\ = \frac{1}{2}\sum_{i}\ P(x_i)\ ln(P(x_i)/Q(x_i))\ +\ \frac{1}{2}\sum_{i}\ Q(x_i)\ ln(Q(x_i)/P(x_i))$; being P and Q the true and approximated likelihoods, respectively.

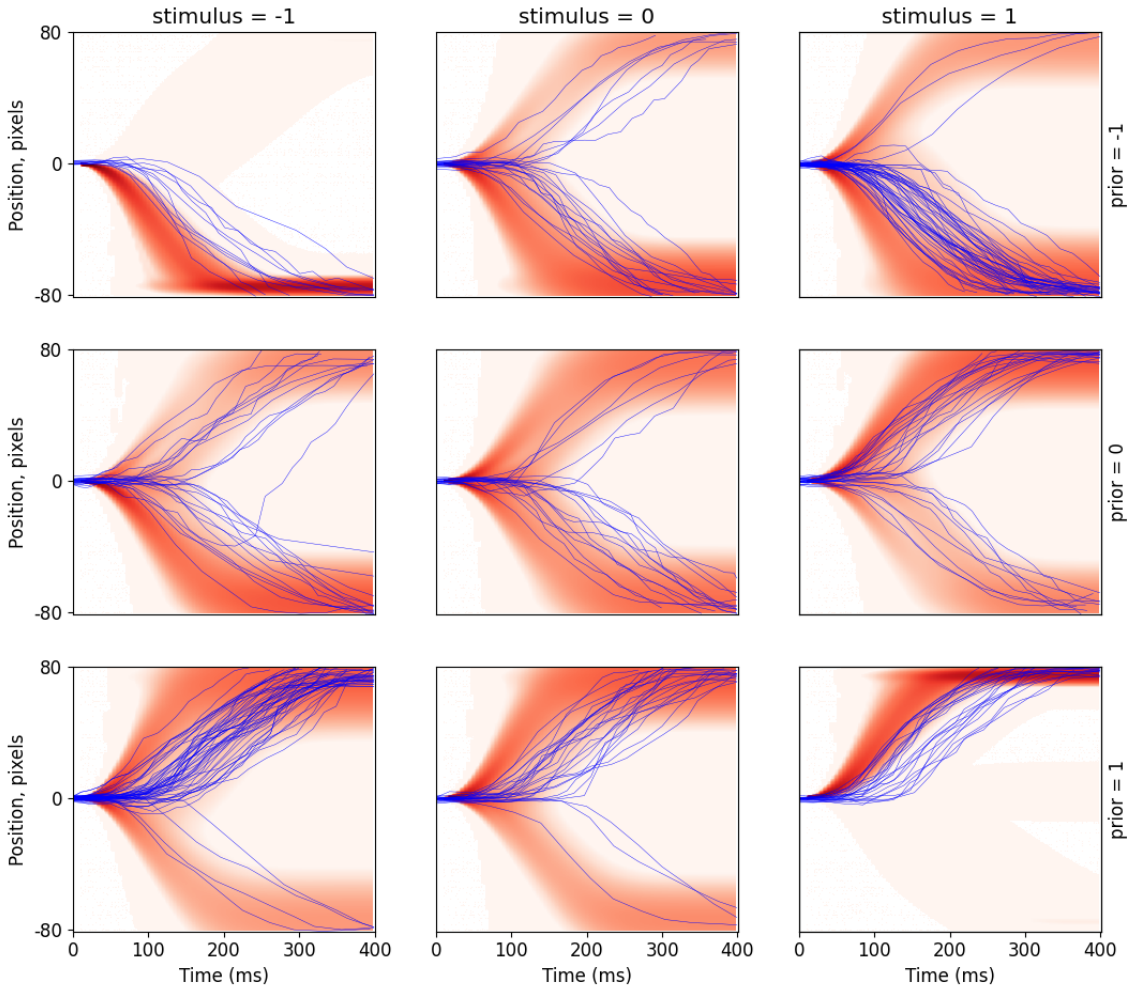

Supplementary figure 6. Rat trajectories for a random subset of 150 trials of animal LE43 (blue curves) plotted over the corresponding model density (red color plot), for different values of stimulus evidence (left column: stimulus=-1; middle column: stimulus=0; right column: stimulus=1) and prior evidence (top row: prior=-1, middle row: prior=0; bottom row: prior=+1). Model densities were obtained by drawing trajectories for 150000 simulated trials with model parameters estimated for the corresponding animal.

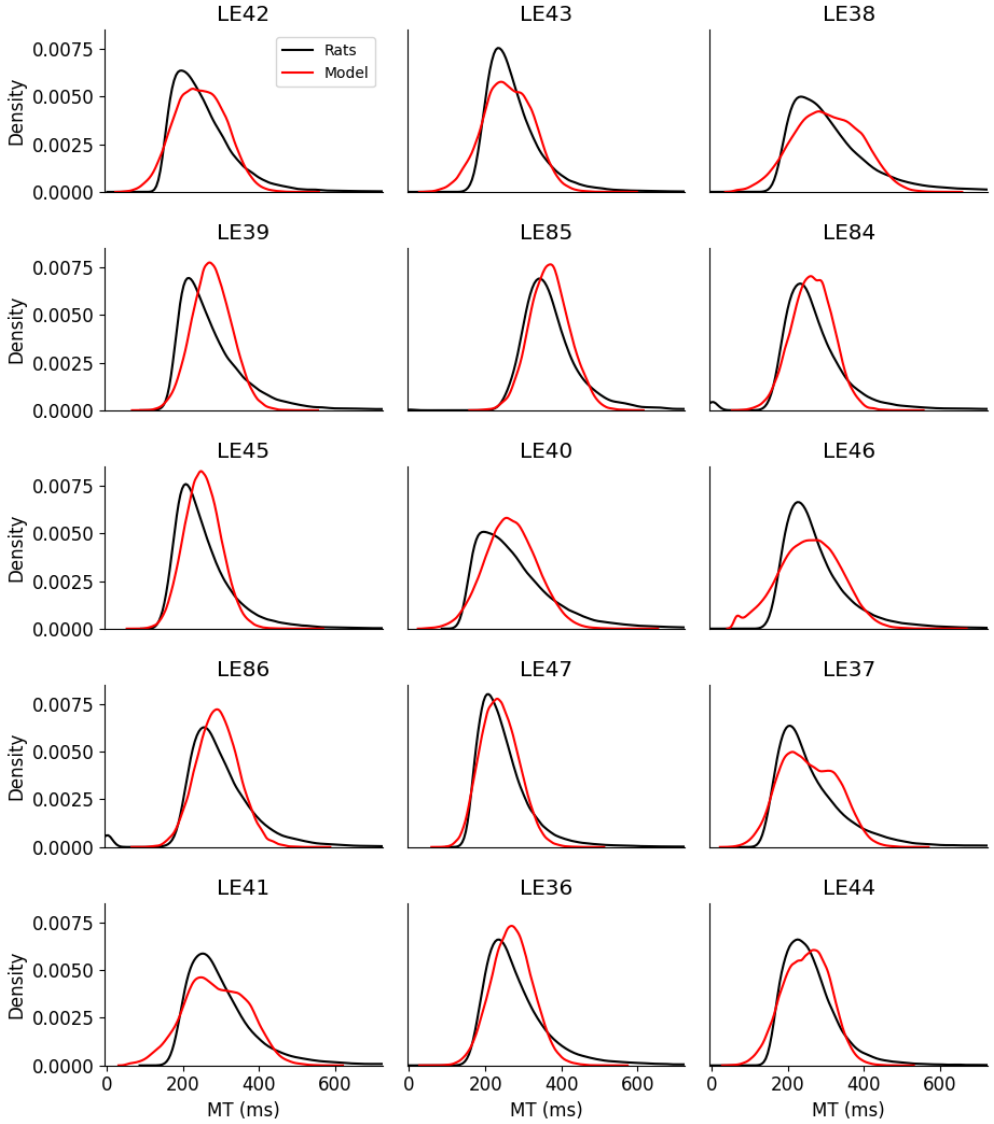

Supplementary figure 7. Rats and model MT distributions of each rat.

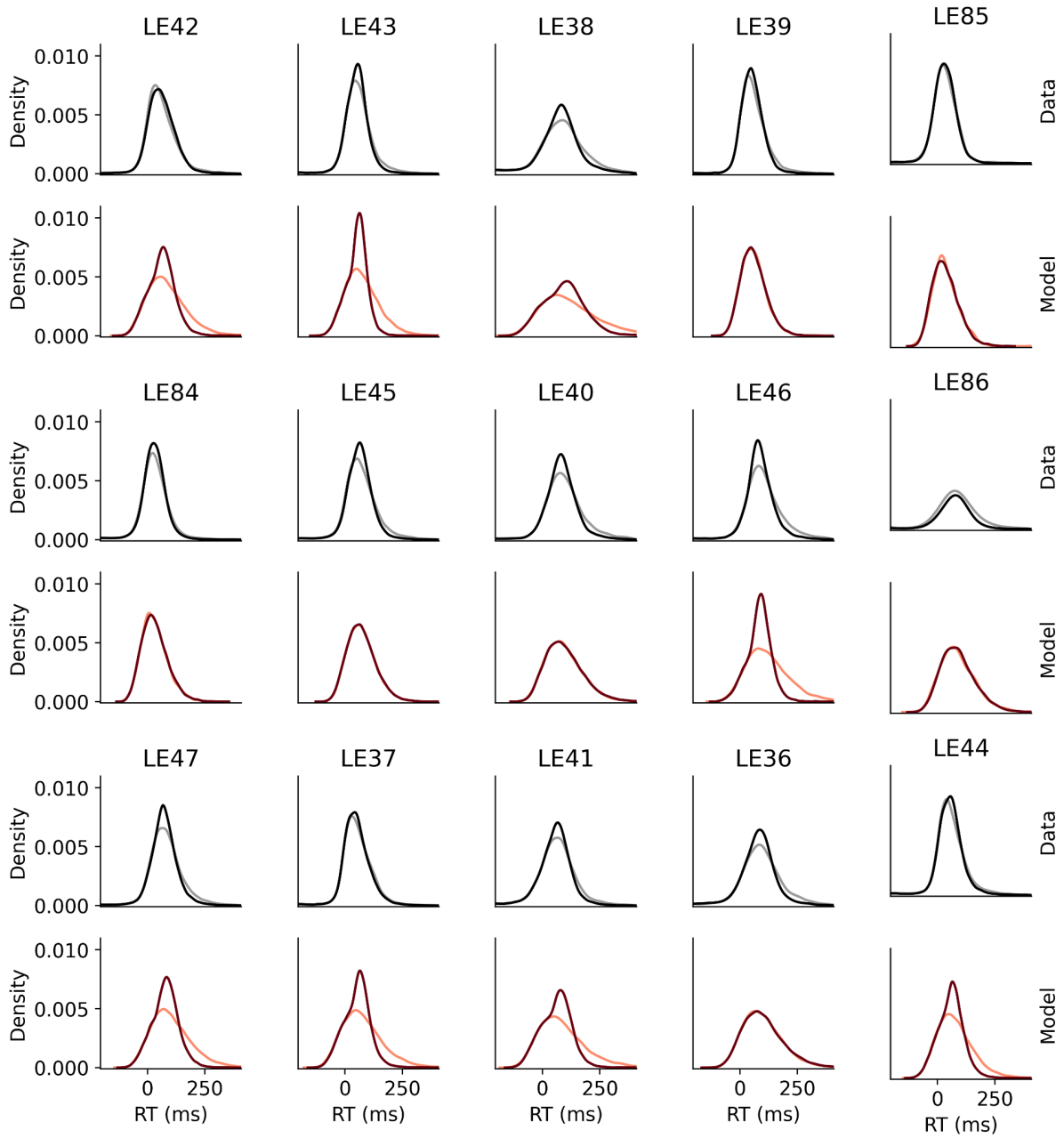

Supplementary figure 8. RT distributions from rats (gray/black lines) and model (orange/brown lines), for different levels of stimulus strength (light: stimulus strength = 0; dark: stimulus strength = 1).

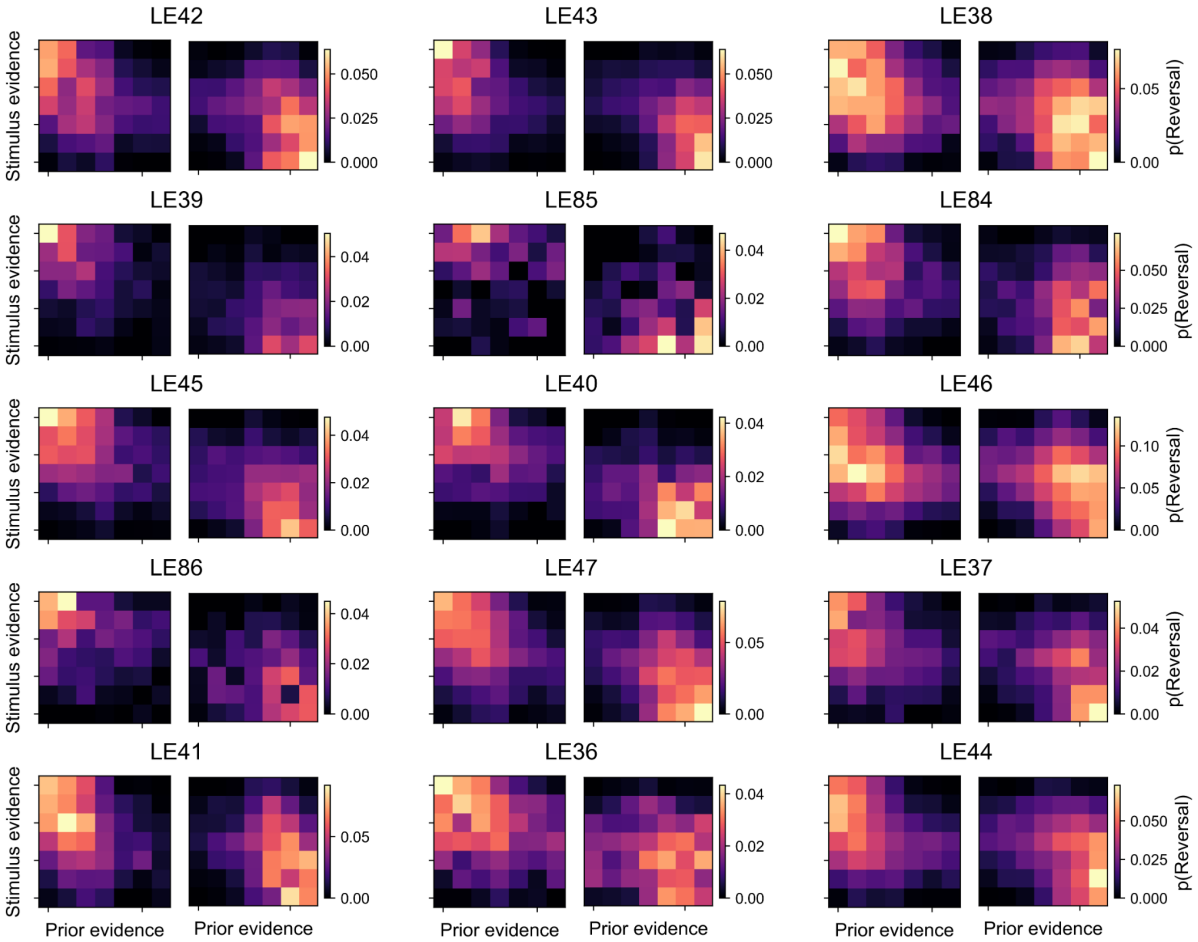

Supplementary figure 9. Proportion of left-to-right reversals (left panels) and right-to-left reversals (right panels) as a function of stimulus and prior evidence, for the model fitted to each individual rat.

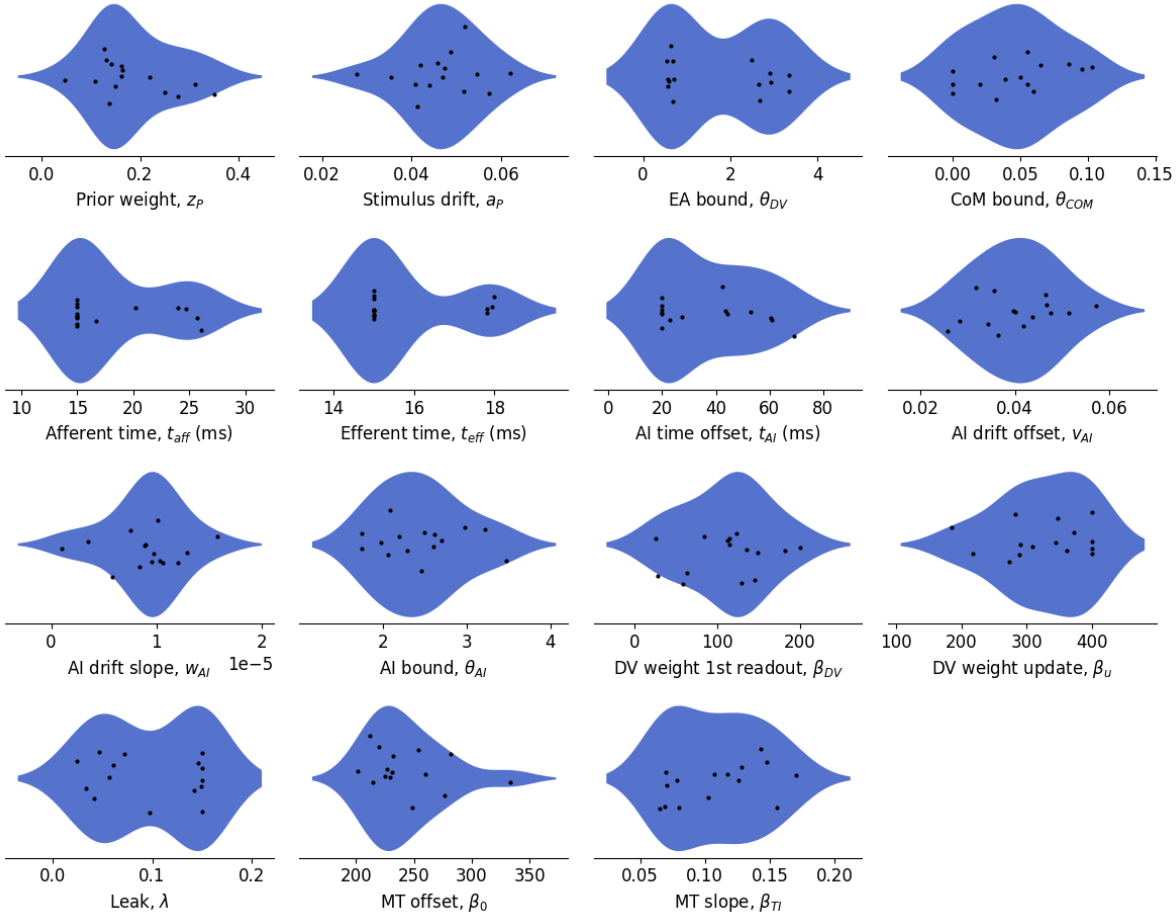

Supplementary figure 10. Fitted parameters for all rats. The parameter of the variance of the MT, σ_{MT}, is not plotted, as it reached the upper bound for all rats (σ_{MT} = 20).